27598

NATIONAL LIBRARY
OTTAWA

CANADA

BIBLIOTHÈQUE NATIONALE
OTTAWA

NAME OF AUTHOR...ANDREW..RODNEY..ALLAN.....

TITLE OF THESIS.REGENERATION...ELECTRODE.....

.IMPEDANCE..ANALYSIS.AND.....

RECORDING.AMPLIFICATION..METHOD...

UNIVERSITY.....ALBERTA.....

DEGREE FOR WHICH THESIS WAS PRESENTED.....M..Sc.....

YEAR THIS DEGREE GRANTED.....1976.....

Permission is hereby granted to THE NATIONAL LIBRARY OF CANADA to microfilm this thesis and to lend or sell copies of the film.

The author reserves other publication rights, and neither the thesis nor extensive extracts from it may be printed or otherwise reproduced without the author's written permission.

(Signed)..R.Allan.....

PERMANENT ADDRESS:

..21..Eagle..Drive

....Sherwood..Park

.....Alberta.....

DATED..February..5...1976

NL-91 (10-68)

INFORMATION TO USERS

THIS DISSERTATION HAS BEEN
MICROFILMED EXACTLY AS RECEIVED

This copy was produced from a microfiche copy of the original document. The quality of the copy is heavily dependent upon the quality of the original thesis submitted for microfilming. Every effort has been made to ensure the highest quality of reproduction possible.

PLEASE NOTE: Some pages may have indistinct print. Filmed as received.

Canadian Theses Division
Cataloguing Branch
National Library of Canada
Ottawa, Canada K1A 0N4

AVIS AUX USAGERS

LA THESE A ETE MICROFILMEE
TELLE QUE NOUS L'AVONS RECUE

Cette copie a été faite à partir d'une microfiche du document original. La qualité de la copie dépend grandement de la qualité de la thèse soumise pour le microfimage. Nous avons tout fait pour assurer une qualité supérieure de reproduction.

NOTA BENE: La qualité d'impression de certaines pages peut laisser à désirer. Microfilmée telle que nous l'avons reçue.

Division des thèses canadiennes
Direction du catalogage
Bibliothèque nationale du Canada
Ottawa, Canada K1A 0N4

THE UNIVERSITY OF ALBERTA

REGENERATION ELECTRODE IMPEDANCE ANALYSIS AND RECORDING AMPLIFICATION METHOD

by

© Andrew Rodney Allan

A THESIS

SUBMITTED TO THE FACULTY OF GRADUATE STUDIES AND RESEARCH

IN PARTIAL FULFILMENT OF THE REQUIREMENTS FOR THE DEGREE

OF MASTER OF SCIENCE

DEPARTMENT OF ELECTRICAL ENGINEERING

EDMONTON, ALBERTA

SPRING, 1976

THE UNIVERSITY OF ALBERTA

FACULTY OF GRADUATE STUDIES AND RESEARCH

The undersigned certify that they have read, and recommend to the Faculty of Graduate Studies and Research, for acceptance, a thesis entitled Regeneration Electrode Impedance Analysis and Recording Amplification Method submitted by Andrew Rodney Allan in partial fulfillment of the requirements for the degree of Master of Science.

.....
Supervisor

.....
Supervisor

.....

.....

.....

Date..Feb 5/76.....

ABSTRACT

A new electrode implant method for recording, simultaneously, the electrical activity from several regenerating nerve fibres is being developed by a physiological research group under the leadership of Dr. R. B. Stein. These implants, called "regeneration electrode units" (REUs) have been successfully used to record nerve impulse activity from the sciatic nerve of the Xenopus laevis during unrestrained leg movement. In the present arrangement, now being tested on cats, several fine silver wire leads run from the REU device to a biologically inert "skin button" containing a multi-pin socket. A multi-channel amplifier arrangement is required to interface the REU to recording and/or prosthesis control systems.

A detailed study of the electrode double layer impedance mechanisms is made to gain data for the amplifier input requirements.

An amplification method to fulfill the interfacing requirements is proposed and tested. The technique provides a means for low noise, interference free transmission of signals from the REU, via long unshielded leads from the drain and source connections of a field effect transistor connected to the REU at the skin socket.

ACKNOWLEDGEMENTS

The research described in this thesis was carried out at the Department of Electrical Engineering and the Department of Physiology, University of Alberta, under the joint supervision of Dr. J. F. Vaneldik and Dr. R.B. Stein, respectively, to whom the author is indebted for their patient assistance and encouragement.

The author would also like to thank Dr. V. Pollak, University of Saskatchewan, for his guidance on the electrode theory of this thesis.

TABLE OF CONTENTS

CHAPTER		PAGE
1	IMPEDANCE THEORY OF METAL ELECTRODES.....	1
	1.1 Introduction.....	1
	1.2 The Regeneration Electrode Unit.....	3
	1.3 Historical Preview of the Electrode Double Layer.....	5
	1.4 Modern Description.....	8
	1.5 Polarizable and Nonpolarizable Electrode Interfaces.....	16
	1.6 The Electrode Impedance.....	23
2	MEASUREMENT OF THE REGENERATION ELECTRODE IMPEDANCE.....	35
	2.1 The Measuring Set-Up.....	35
	2.2 Measured Results.....	38
	2.3 Implications for the Recording Amplifier.....	45
3	REGENERATION ELECTRODE AMPLIFIER.....	51
	3.1 General.....	51
	3.2 Amplification Method.....	51
	3.3 D.C. Analysis.....	52
	3.4 A.C. Analysis.....	56
	1. Representing the FET.....	56
	2. Voltage gain at the FET drain and source.....	56
	3. Input stage voltage gain.....	60
	4. The op-amp stages and circuit feedback.....	63
	3.5 Amplifier Noise Mechanisms.....	66

CHAPTER PAGE

3.6 Active Device Noise Considerations... 68

3.7 Amplifier Noise Measurements..... 73

4 AMPLIFIER RECORDING TESTS..... 84

4.1 Preparation..... 84

4.2 Tests..... 84

4.3 Suggestions for Interference Noise Level Reduction..... 87

5 DISCUSSION..... 91

5.1 Electrode Impedance..... 91

5.2 Amplification Method..... 93

BIBLIOGRAPHY..... 96

APPENDIX I BRIDGE APPROXIMATION..... 99

APPENDIX II COMPARATIVE MEASUREMENTS ON THE GRASS P15 PHYSIOLOGICAL AMPLIFIER..... 103

LIST OF FIGURES

FIGURE		PAGE
1.1	Cross-sectional view of a single regeneration electrode unit hole.....	6
1.2	The electrode-saline double layer.....	9
1.3	Double layer potential profiles.....	15
1.4	Double layer energy barrier.....	18
1.5	Normalized exchange current density vs. overpotential.....	21
1.6	Transmission line equivalent circuit of the Warburg Impedance.....	30
1.7	Equivalent circuit of electrode impedance.	32
2.1	Schematic diagram of set-up used to measure the electrode impedance.....	37
2.2	Impedance characteristic of a single REU lead.....	39
2.3	Impedance characteristic of a single 76 micron teflon coated silver wire.....	41
2.4	Impedance characteristics of 6 REU leads..	42
2.5	Average impedance characteristics of 6 REU leads.....	43
2.6	Impedance characteristic of a pair of implanted REU leads.....	44
2.7	X-ray photograph of implanted regeneration electrode unit in the leg of a cat.....	46
2.8	Amplifier-source equivalent input circuit.	49
3.1	Amplifier circuit diagram.....	53
3.2	FET transconductance in the "ohmic" region.....	57
3.3	(a) FET represented in-circuit	
	(b) The small signal equivalent circuit..	58

FIGURE		PAGE
3.4	(a) A.C. pathway of transistor Q_2 illustrating common base configuration	
	(b) The low-frequency approximate hydrid equivalent circuit.....	58
3.5	(a) A.C. pathway of amplifier input stage	
	(b) Equivalent circuit of same.....	61
3.6	Differential a.c. coupled op-amp stage....	64
3.7	Voltage-series feedback of input circuit..	64
3.8	Contours of constant narrow band noise figure for the Fairchild 2N3117 bipolar transistor.....	72
3.9	Normalized current gain vs. collector current for the Fairchild 2N3117 bipolar transistor.....	72
3.10	Amplifier equivalent input noise model....	75
3.11	Amplifier noise measurement circuit.....	78
3.12	Equivalent input noise vs. source resistance - REU amplifier.....	80
3.13	Noise figure vs. source resistance - REU amplifier.....	82
4.1	Recording preparation showing dorsal cutaneous nerve lifted into paraffin onto a silver recording electrode.....	85
4.2	Amplifier test recordings.....	86
4.3	Single nerve impulse with baseline disrupted from 60 Hz external interference	88
4.4	Suggested circuit to give common mode rejection.....	90

FIGURE		PAGE
AII.1	Oscilloscope photograph of several superimposed nerve impulses.....	104
AII.2	Amplifier output noise envelope.....	104
AII.3	Equivalent input noise vs. source resistance - Grass P15 Amplifier.....	105
AII.4	Noise figure vs. source resistance - Grass P15 Amplifier.....	105

CHAPTER 1

IMPEDANCE THEORY OF METAL ELECTRODES

1.1 Introduction

Metal electrodes are extensively used for the extracellular investigation of neural electrical activity. Simply speaking, the electrodes are used to conduct to the recording apparatus, the potential variations caused by extracellular ionic currents responding to nerve action potentials. The recently devised regeneration electrode unit (REU) described in Section 1.2, is a specialized electrode involving an array of ten or more silver electrodes.

Electrode impedance is significantly complicated by the interface between the electrode metal surface and the electrolytic solution surrounding the body tissue. When the electrode is placed in contact with the electrolyte, electrochemical reactions occur at the interface. The passage of charge across the interface produces a charge separation causing the impedance to become capacitive. Because the surface area of the REUs is small (approximately 5×10^{-5} cm^2), the interface impedance will contribute a significant amount to the total electrode impedance. In addition to the aforementioned interface capacitance, there is a diffusion process present when an external electric field is applied to the electrode. As a result of this diffusion process, the electrode impedance resulting will display an R-C characteristic that is distributed rather

than lumped. Normally, with larger electrodes, these mechanisms are less significant in comparison to the resistance from the bulk of the solution and they are ignored. They cannot be ignored however in the case of small electrodes.

To further complicate matters, the impedance mechanisms depend considerably upon the metal type and the electrolyte ingredients and concentration. Voltage-dependent non-linearities in the mechanisms may also severely distort the externally applied signals and affect the recording results. Consequently, the electrical characteristics of the electrode play an important role in deciding upon the recording amplifier input specifications. Considerations of particular importance are those of impedance magnitudes, frequency dependence, amplitude non-linearities; electrode shunt capacitance; electrode physical requirements and also the electrode-amplifier noise requirements. As an example, the impedance magnitude will play an important part in determining whether the amplifier input device should be a bipolar transistor or a field effect transistor.

The subsequent sections of this chapter attempt to bring together much of the widely scattered information on electrode theory found in electrochemistry papers and text-books, thus providing a more thorough understanding of the electrode-saline interface. It is hoped, that in addition to supplying information needed to specify the amplifier

input requirements to accept the regeneration electrode unit, the information will be of value towards providing a more rational approach to the REU's fabrication and use, (i.e. in terms of specifying predictable and consistent impedance levels for the electrodes). This will prove to be of particular value as far as impedance matching of the electrodes to the amplifier is concerned. Reproducible and reliable nerve signals will be required, particularly if the REU proves to be a worthwhile device for neural control of artificial limbs. Consistent electrode impedance will also be of value during differential recordings where balancing of source impedance is necessary to optimize the common mode rejection of the amplifier.

The electrode impedance theory of this chapter will be applied in obtaining measurement information on the impedances of the REU devices in chapter 2. An equivalent circuit of the input source is made in order to specify the input properties of the recording amplifier. In the remaining chapters a viable method of amplification of the REU signal will be discussed and tested.

1.2 The Regeneration Electrode Unit

This device has been developed to record impulses from many nerve fibres simultaneously with the same device. It is called a Regeneration Electrode because it relies solely upon the regeneration of peripheral nerves through it for its operation. The device basically consists of a number of parallel cylindrical holes (10 holes at present)

approximately 100 microns in diameter drilled perpendicularly through a flat epoxy plate (for construction and structure details refer to Mannard, Stein and Charles, 1974). A hole is drilled so that it intersects at right angles through a 76 micron diameter silver wire embedded midway in the thickness of the epoxy slab. The silver wires are placed as close together as is technically possible.

The device is then inserted between the two ends of a cut nerve so that during regeneration some of the nerve fibres will grow through the holes. Thus, a passing nerve spike will generate a potential difference across the resistance of the extracellular fluids, contained between the center and the outside of the hole. If the fluid outside the hole is held at ground potential the wire at the center of the hole will act as an electrode and records a triphasic (Stein and Pearson, 1971) action potential.

It has been predicted (Stein, R. B. in private communication) that the recorded signal strength at the electrode will be about 50 microvolts peak amplitude. The triphasic peak amplitude is given by (Stein and Wong, 1970)

$$V_s = C\left(\frac{L}{D}\right)^2 \qquad (1.1)$$

where L is the length of the hole, D is the hole diameter and C is an empirical proportionality constant that is temperature dependent. Typically L is 1 mm. with optimization between signal strength and ionic diffusion.

A cross-sectional view of a single hole is illustrated in Fig. 1.1.

The resistance across which the recorded potential will develop may be predicted for low frequencies from:

$$R = \frac{R'}{2}$$

$$= \frac{1}{2} \rho \frac{\frac{L}{2}}{\pi (\frac{D}{2})^2}$$

$$\text{giving,} \quad R = \frac{\rho L}{\pi D^2} \qquad (1.2)$$

where ρ is the fluid resistivity which is near 100 ohm-cm. for Ringer solution. Thus, resistances in the order of 30 kilohms are expected. The impedance, due to the saline-silver interface, however, is much more complicated, and requires special attention as non-linear frequency dependence may affect electronic amplification of the electrode signals.

1.3 Historical Preview of the Electric Double Layer

When a metal is placed into a solution there will exist a potential difference across the metal-solution interface. Nernst in 1889 (discussed in Butler, 1951) explained this phenomenon as being due to the difference between the solution pressure of the metal and the osmotic pressure of the ions in the solution. If the difference favoured the solution, the solution ions will be forced to adhere to the surface of the metal to form a thin layer (a process presently known as adsorption). This will continue

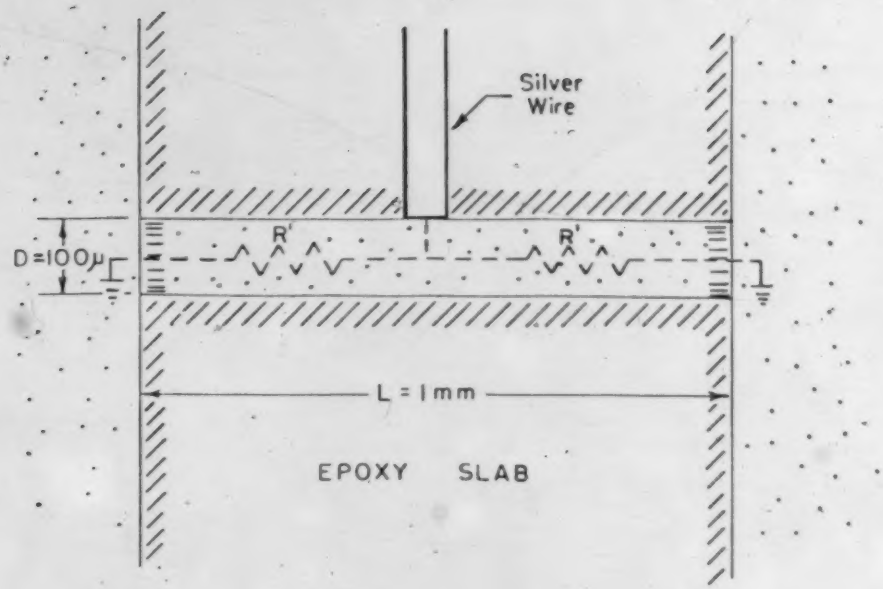

Figure 1.1 Cross-sectional view of a single regeneration electrode unit hole.

to happen, until the electric forces due to the unbalanced charges are in equilibrium with the pressure difference. Thus, there will exist at the immediate vicinity of the interphase a separation of ionic charges called an ionic double layer. Helmholtz (discussed in Butler, 1951, Chapter 1 and 2; Davies, 1967) treated this charge separation as a capacitor. If a charge per unit area σ on each plate of the capacitor is separated by a distance d the capacitance of the double layer is predicted by:

$$C = \frac{\sigma}{\phi}$$

giving, $$C = \frac{\kappa}{4\pi d}$$

where κ is the dielectric constant of the medium and ϕ is the potential difference between the plates. This however predicts capacitances much higher than those measured experimentally.

The Guoy-Chapman model (Davies, 1967; Butler, Chapter 2, 1951; Delahay, 1965) later compensated for the thermal and mechanical mobility of the liquid ions. This model pictured a rigid layer of ions on the metal side of the interphase and a diffuse layer on the solution side. The concentration of ions decreased in an exponential fashion with distance away from the interphase. An approximate expression for the concentration distribution for ions, which do not display any specific preference to the metal with which they are placed in contact, follows a Boltzmann distribution (Delahay, 1975), thus:

$$C = C_s e^{-\frac{\phi z q}{kT}} \qquad (1.3)$$

where C is the concentration of ions at a point in the diffusion layer where the potential is ϕ, C_s is the concentration of ions in the bulk solution, z is the valency of the ions, k is Boltzmann's constant (= 1.38×10^{-23} joules/molecule ^{o}K), T is the absolute temperature and q is the electronic charge (= 1.6×10^{-19} coul). In 1924 Stern (Davies, 1967; Butler, Chapter 2, 1951; Delahay, 1965) combined the double layer models of Helmholtz, Guoy and Chapman. He proposed part of the charge to be firmly bound to the metal surface and the rest of the charge to be loosely bound and exist as a diffuse layer. This picture as modified by Grahame (Grahame, 1947) is the presently accepted model of the double layer and will be the basis of the remaining discussion of the subject. There are many recent refinements to the theory, but these will be largely bypassed as they will not offer any dramatic changes in the theory needed to describe the impedance characteristics of an electrode.

1.4 Modern Description

The double layer in equilibrium is described in two regions as shown in Fig. 1.2. Immediately adjacent to the solid surface is the compact layer, or inner layer, only a few molecular diameters in thickness. Following this layer is the diffuse layer, or outer layer, of molecules which decreases in concentration out towards the bulk solution.

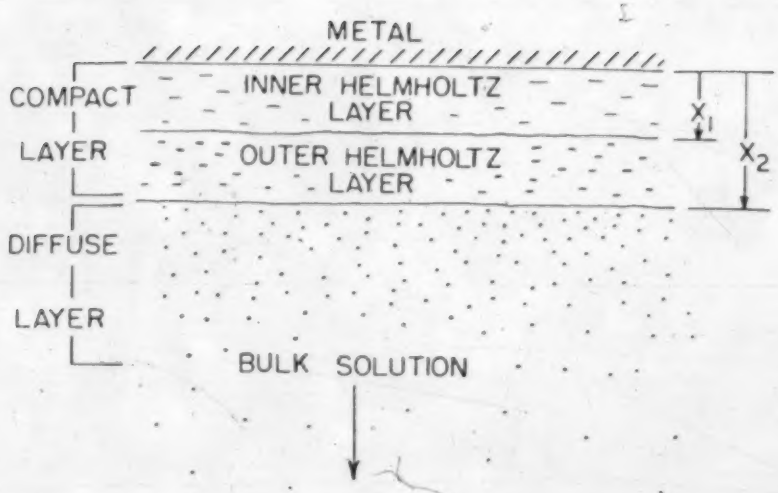

Figure 1.2 The electrode-saline double layer.

Since the entire interphase system is electrostatically neutral, there must also exist on the surface of the metal an excess or deficit of electronic charge imposed by the charge transfer during the adsorption process.

Depending on the electrochemical properties of the different ions in solution, it is generally found that in most solutions there are specific ions and sometimes even neutral substances that will show a specific preference for adsorption and will cling tightly to the metal surface. (Delahay, 1965, P. 58, states that any ion can be specifically adsorbed under favorable polarity and magnitude of charge on the electrode surface). The exact reason for this "specific adsorption" is still controversial. Normally, an ion in solution is surrounded by attracted water molecules forming a hydration sheath. Forces, other than electrostatic attraction called London Forces, exist that may act on the ion causing it to penetrate the hydration sheath boundary and stick directly to the metal surface. The degree of hydration then would determine whether an ion could get close enough to the metal surface to be specifically adsorbed. It is generally agreed that the specific adsorption forces are short range forces. Grahame has suggested that the forces may be due to a form of covalent bonding at the metal surface. Also ions with hydrophobic ends would receive less resistance to their approach to the metal surface.

If an ion does not display specific adsorption tendencies toward the metal, then the forces of attraction

will not be great enough to separate the ion from its hydration sheath, and the ions will form a second layer behind the specifically attracted ions. This layer is called the outer Helmholtz layer. Thus, the compact layer may actually consist of two sub-layers. Usually the inner Helmholtz layer consists of anions because of their greater polarizability and compressibility.

In its modern form the compact layer is modelled as two discrete parallel layers of opposite charges, the innermost layer generally being a compact regular array of anions held in place by strong close range forces. At the outermost layer the forces will not act as strongly and thermal vibration will somewhat disrupt the regular array of cations. Due to this separation of charge there will be an electric potential appearing across the compact layer. Assuming a uniform dielectric constant κ across the compact layer and neglecting the thermal diffusion of the outermost layer, Ershler and Grahame (Delahay, PP. 68 to 73, 1965; Grahame, 1947) estimated this potential as:

$$\phi_M - \phi_{x_2} = \frac{4\pi q_1 (x_2 - x_1)}{\kappa} \qquad (1.4)$$

The term $\phi_M - \phi_{x_2}$ denotes the potential difference between the metal surface and the outermost limit of the second sublayer of the compact layer. Distance to the locus connecting the electrical centers of the inner Helmholtz layer is x_1 and to the centers of the outer Helmholtz layer is x_2. The potential is considered to be entirely

due to the charge q_1 of the inner Helmholtz layer, and the diffuse layer adjoining the compact layer has been considered as completely polarizable.

When adsorption of ions is nonspecific the forces involved will be due to coulombic and chemical bonding effects. As already mentioned, these ions will not be able to approach the electrode surface any closer than the outer Helmholtz plane, as they will be separated from the inner Helmholtz plane or surface of the metal by a layer of water of solvent molecules. At this plane the concentration of ions will be maximal and compact. Moving away from this compact layer towards the bulk solution, thermal agitation will have an increasing tendency to overcome coulombic forces, and will disrupt the molecular organization until finally it is the primary disturbance. This region is called the diffuse layer.

The diffuse layer ions behave as an "ionic atmosphere" surrounding the electrode and have been described by the Debye-Huckel equations (Butler, Chapter 2, 1951; Grahame, 1947). Poissons equation is used to describe the potential variation ϕ along one direction x perpendicular to the electrode surface:

$$\frac{d^2\phi}{dx^2} = -\frac{\rho}{\varepsilon} \qquad \{1.5\}$$

The permittivity of the solution is ε and ρ the charge per unit volume is determined by the sum:

$$\rho = \Sigma n_i z_i q \qquad \{1.6\}$$

where n_i is the number of ions per unit volume at the

position where the potential is ϕ and $z_i q$ is the charge of the ion. An expression for n_i is obtained from the Boltzmann Distribution equation as:

$$n_i = n_{oi} e^{-\frac{W_i}{kT}} \qquad \{1.7\}$$

where W_i is the work required to bring an ion from the bulk of the solution to the potential ϕ, k is the Boltzmann constant, T is the absolute temperature and n_{oi} is the number of ions per unit volume in the bulk of the solution. Hence:

$$\rho = \Sigma n_{oi} z_i q e^{-\frac{W_i}{kT}} = \Sigma n_{oi} z_i q e^{-\frac{z_i q \phi}{kT}} \qquad \{1.8\}$$

since $W_i = z_i q \phi$ the electric work done on the ion. Substitution of Eq. {1.8} into Eq. {1.5} gives:

$$\frac{d^2\phi}{dx^2} = \frac{-q}{\epsilon} \Sigma n_{oi} z_i e^{-\frac{z_i q \phi}{kT}} \qquad \{1.9\}$$

Solving this equation from $\phi(x)$ involves integration of the following expression (Grahame, 1947):

$$\int_{x_s}^{x} dx = -\left[\frac{q}{8kTn_o}\right]^{\frac{1}{2}} \int_{\phi_s}^{\phi} \operatorname{csch} \frac{zq\phi}{2kT}\, d\phi \qquad \{1.10\}$$

where x_s is the distance out to the bulk solution and we define ϕ_s the potential of the bulk solution as zero potential. Integration gives:

$$x' = x - x_s = -\left[\frac{\epsilon kT}{2z^2 q^2 n_o}\right]^{\frac{1}{2}} \ln \tanh \left[\frac{zq\phi}{4kT}\right] \qquad \{1.11\}$$

Defining the Debye reciprocal length as:

$$\ell = \left[\frac{2z^2 q^2 n_o}{\varepsilon kT} \right]^{\frac{1}{2}}$$

then, $$x' = \frac{1}{\ell} \ln \tanh \left[\frac{zq}{4kT} \phi \right] \qquad \{1.12\}$$

or, $$\phi = \pm \frac{4kT}{zq} \text{ arc } \tanh e^{-\ell x'} \qquad \{1.13\}$$

For low concentration solutions this expression may be approximated as:

$$\phi = \pm \frac{4kT}{zq} e^{-\ell x'} \qquad \{1.14\}$$

If the solution contains only nonspecifically adsorbed ions, the charge per unit area on the metal electrode surface q_M will be balanced by an equal and opposite charge per unit area $-q_M$ contained in the diffuse layer. However, if specific adsorption is present, the diffuse layer will contain an additional charge density q_s balancing the excess charge density due to specifically adsorbed ions in the inner Helmholtz plane. The charge per unit area of surface charge density is defined as:

$$q = \int_x^\infty \rho \, dx \qquad \{1.15\}$$

and is the total charge contained in a column of solution extending from the plane of discontinuity into the bulk solution where $\phi = 0$.

Potential profiles of the entire double layer are shown in Fig. 1.3. Fig. 1.3(a) is the case where the adsorbed charge in the compact layer is less than the charge

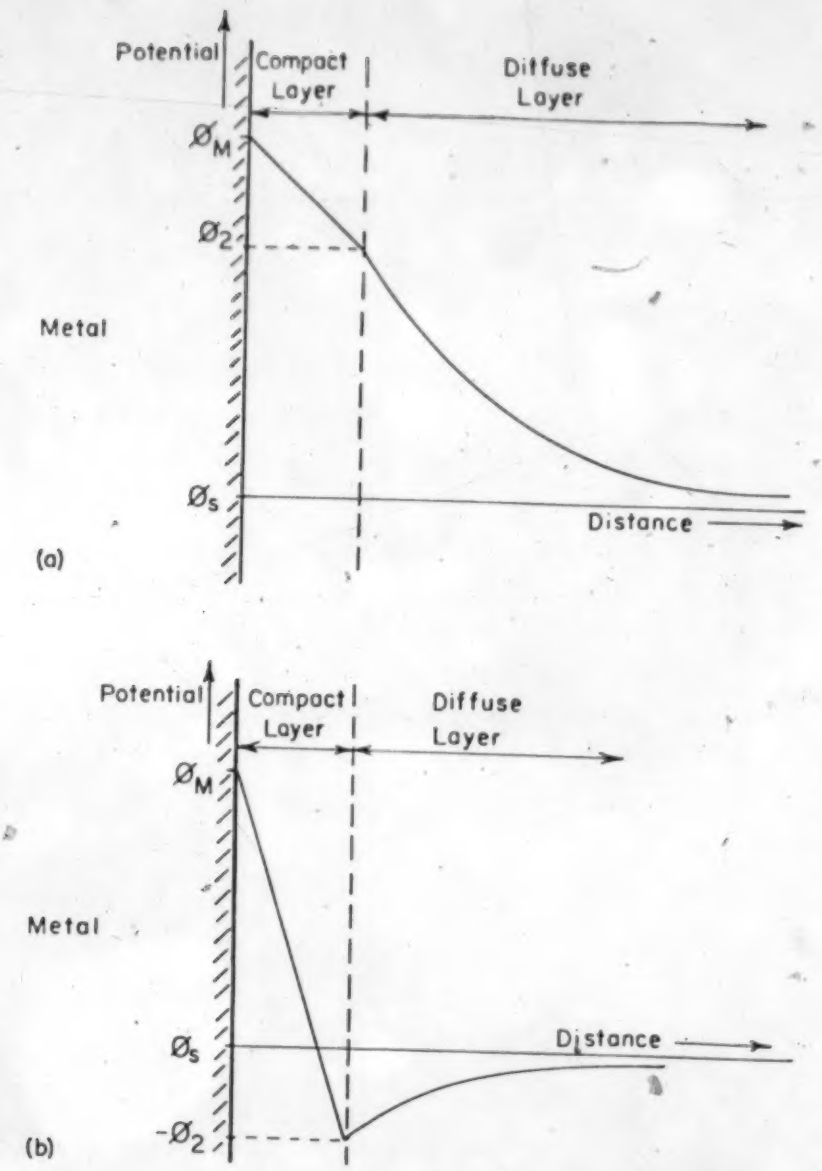

Figure 1.3 Double layer potential profiles (a) when the compact layer charge is less than metal surface charge, and (b) when the compact layer charge is greater than the metal charge.

on the metal surface, while Fig. 1.3(b) is the case where very strong adsorptive forces collect a charge that is greater than the metal charge. The potential across the compact layer is approximated as having a linear dependence (Eq. (1.4)) on the distance from the surface. Although this does not create a serious error, it is clear that the dependence is more complex due to changes with distance of the dielectric constant of the medium (Parsons, P. 166, 1954).

1.5 Polarizable and Nonpolarizable Electrode Interfaces

If an external potential difference is applied between a metal electrode and the bulk solution into which it is immersed, and no flow of charge occurs across the interface boundary, the electrode is said to be behaving as an ideally polarizable electrode (Mohilner, 1966; Breyer, 1963; Davies, 1967; Parsons, 1954; Parson, 1970: Bockris and Reddy, 1970). The behavior is entirely governed by the separation of charge in the double layer, and the potential difference gradient across the interface is easily changed by the external power source. This action is analogous to charging a non leaky capacitor. The equilibrium attained is an electrostatic equilibrium of separated balanced charges. Current flow will be entirely a displacement current that will irreversibly polarize the interface. On the other hand, if charge can freely migrate across the interface, and despite the current flow the interface layer does not wander away from its equilibrium potential gradient, the electrode will behave as an ideally

nonpolarizable electrode. This action would be similar to that of applying an external potential difference to a shorted capacitor.

Real electrodes which can satisfy either of these ideal extremes of course do not exist, as polarizable electrode interfaces will leak current to some extent and nonpolarizable interfaces will change their potential slightly. Distinction is made only in the relative degrees of polarizability. The degree of polarizability of an electrode interface is governed by electrochemical faradaic processes in the form of oxidation and reduction reactions, which control the rates at which charges can transfer across the interface boundary.

Fig. 1.4 shows a simplified representation of the activation energy barrier that an electron must tunnel through during such a charge transfer reaction. The height of the activation energy barrier that the electron sees on the solution side during the oxidation reaction is given by the product of the metal work function $-q\Delta\phi$ and the barrier symmetry factor β. $\Delta\phi$ is the potential difference required to remove the electronic charge, $q = 1.59 \times 10^{-19}$ coulomb, from the metal surface and β is defined by

$$\beta = \frac{\text{Distance across double layer to energy barrier peak}}{\text{Total distance across double layer}}$$

Conversely, the energy barrier height the electron sees during the reduction reaction (seen from the metal side of the double layer) is $(1-\beta)\, q\Delta\phi$. Thus, application of an

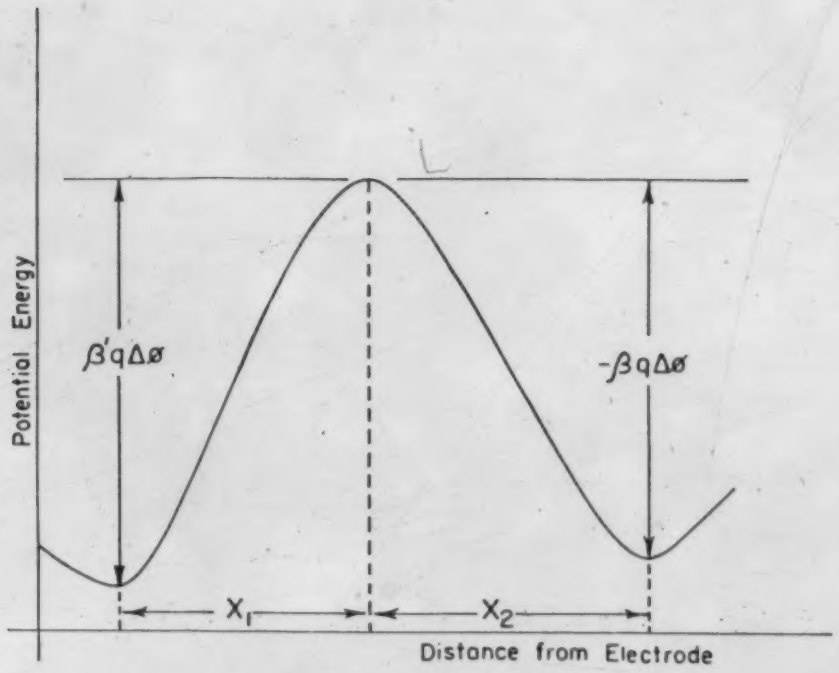

Figure 1.4 Double layer energy barrier that electrons must surmount during electrode reactions. The symmetry factor β is determined by the ratio:

$$\beta = \frac{X_2}{X_1 + X_2}$$

and β' by $\beta' = \frac{X_1}{X_1 + X_2} = (1 - \beta)$.

external EMF will have the effect of increasing the energy barrier in one reaction direction while decreasing it in the other.

When no external EMF is applied to the electrode a stand off condition exists between the oxidation and reduction exchange current rates, and a net compromising equilibrium exchange current density j_o will exist giving rise to an equilibrium potential difference across the interface. This phenomenon is similar to the contact potential difference experienced at the junction of two dissimilar metals. Upon application of an EMF however, a nonequilibrium current density j is created due to a difference in the oxidation and reduction exchange rates, and the interface potential difference will depart from its equilibrium value by an amount E called the nonequilibrium overpotential. The relationship between j and E can be determined by the Butler - Volmer equation of electrodics (Bockris and Reddy, 1970):

$$j = j_o\left(e^{(1-\beta)\frac{Eq}{kT}} - e^{-\beta\frac{Eq}{kT}}\right) \qquad (1.16)$$

where q is the electronic charge, k is Boltzmann's constant and T is the absolute temperature. In most cases where electrodes display little current rectification tendencies (an effect known as faradaic rectification) the symmetry factor, β, will take on an approximate value of $\frac{1}{2}$, thus Eq. (1.16) becomes:

$$j = j_o\left(e^{\frac{qE}{2kT}} - e^{-\frac{qE}{2kT}}\right)$$

or, $$j = 2 j_o \sinh \frac{qE}{2kT} \qquad \{1.17\}$$

Hence equal positive and negative overpotentials will produce equal exchange currents, as shown in Fig. 1.5.

When expanded in a series Eq. {1.17} may be reduced to a linear approximation of the form:

$$j = j_o \frac{qE}{kT} \qquad \{1.18\}$$

when $\frac{qE}{kT} < 1$ or $E < 26$ mv at room temperature. As an example, at $E = 20$ mv, percent error in the linear approximation will be -2.5%. This linear dependence between current density and overpotential indicates an ohmic behaviour of the electrochemical reaction currents at low externally applied voltages. We may rewrite Eq. {1.18} as;

$$E = \rho_{MS} j$$

where $\rho_{MS} = \frac{kT}{qj_o}$ is the metal-solution interface resistivity. Close examination of this resistivity identity:

$$\rho_{MS} = \frac{\partial E}{\partial j} = \frac{kT}{qj_o} \qquad \{1.19\}$$

reveals the polarizability of the electrode interface to depend on the magnitude of the equilibrium exchange current density j_o. As j_o increases to very large values:

$$\lim_{j_o \to \infty} \rho_{MS} = \lim_{j_o \to \infty} \frac{\partial E}{\partial j} = 0$$

the interface becomes ideally conductive and tends towards ideal nonpolarizable electrode behavior. If on the other hand j_o becomes very small:

$$\lim_{j_o \to 0} \rho_{MS} = \infty$$

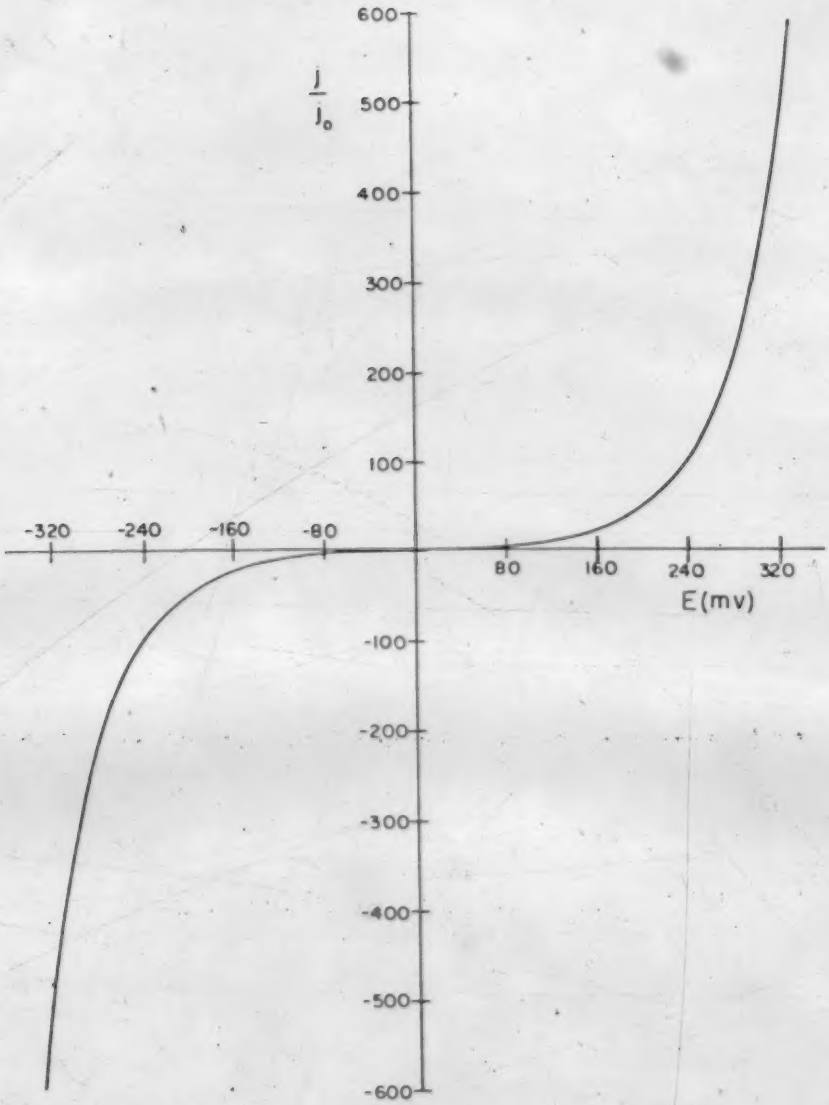

Figure 1.5 Normalized exchange current density versus overpotential.

and the electrode interface approaches ideally polarizable behavior.

As an example, consider a pure silver electrode immersed in an aqueous solution of potassium and chloride ions. A conceivable process would be the flow of silver ions into solution and the reaction:

$$Ag \rightleftharpoons Ag^{+} + e^{-} \qquad \{1.20\}$$

However, the activation energy is large so that only a small exchange current would result. The discharge of solution ions into the metal is not likely to occur and so the electrode behaves as a polarizable electrode.

If the silver electrode was instead immersed into an aqueous solution of silver chloride it would behave quite differently. The reaction {1.20} occurs readily and quickly, and will transfer considerable charge due to the silver ions already present in the solution. Here the electrode behaves as a nonpolarizable electrode.

A polarizable electrode may be converted into a nonpolarizable electrode by creating an adherent layer of salt on its surface. An example of such an electrode is the silver-silver chloride electrode in which a layer of silver chloride is produced on a wire by electro-deposition. When immersed into a chloride solution, and an external potential is applied, the reaction will be:

$$Ag + Cl^{-} \rightleftharpoons AgCl + e^{-} \qquad \{1.21\}$$

If the metal is placed at a positive potential with respect to the solution, silver ions on the surface will

extract chloride ions from the solution. When the potential is reversed, chloride ions will be discharged into solution.

1.6 The Electrode Impedance

Now equipped with a better picture of the electrode double layer process, we are in a position to formulate the impedance pathway that influences electrode current flow response to externally applied voltages. Starting with the electrode metal interior the current flow will encounter a small resistance which we will denote as R_M. Then, once reaching the interface boundary, the impedance will depend largely on the polarization of the double layer and the magnitude of the excitation voltage. Two pathways are available, these being the capacitive and conductive pathways. If the electrode is highly polarizable the impedance behavior will mostly depend on the separation of charge across the double layer boundary. This capacitive influence, which we will call C_{DL}, is voltage dependent if the excitation amplitude is large (Bockris and Reddy, 1970) but remains fairly constant at lower amplitudes with magnitudes in the order of 10 to 20 $\mu F/cm^2$. Alternatively, the electrode may be highly nonpolarizable causing the impedance to depend on the conductive exchange current reactions across the double layer. When excitation voltage is low the resistivity behaves linearly according to Eq. {1.18}:

$$\rho_{MS} = \frac{kT}{qJ_o} , \qquad \{1.22\}$$

thus allowing undistorted passage of exchange current. Differentiation of Eq. {1.17} gives the incremental high voltage resistivity as:

$$\rho_{MS} = \frac{\partial E}{\partial j}$$

$$= \frac{kT}{qj_o} \operatorname{sech} \frac{qE}{2kT}$$

$$\text{or,} \quad \rho_{MS} \approx \frac{2kT}{qj_o} e^{-\frac{qE}{2kT}} \qquad \{1.23\}$$

when $\frac{qE}{kT} >> 1$ or $E >> 26$ mv

which indicates that severe distortion of current will result at high voltage if the double layer impedance comprises a large portion of the net electrode impedance. Resistance due to the exchange current resistivity will be designated as R_{DL} and will be combined in parallel with C_{DL} since the interface must support both currents simultaneously (especially when behavior is somewhere midway between the polarizable and nonpolarizable extremes).

Temporarily bypassing the diffusion zone and focusing attention on the bulk solution, the conduction process here is a result of electrolyte ion drift responding to the externally applied electric field. The impedance therefore, will demonstrate ohmic behavior (Bockris and Reddy, 1970) and at low frequencies may be represented as a pure resistance, R_S.

Returning now to the diffusion zone, we find that due to its frequency dependence the impedance cannot be

represented in any simple manner as it is a distributed parameter system due to the ionic diffusion. The charge transfer process in salt solutions is diffusion controlled and is described by Fick's Diffusion Law for large flat surfaces (Margaretha, 1970; Bockris and Reddy, 1970; Grahame, 1952; Bockris, 1954; Randles, 1947)

$$\frac{\partial c(x,t)}{\partial t} = D \frac{\partial^2 c(x,t)}{\partial x^2} \qquad \{1.24\}$$

where c(x,t) is the ion concentration dependent on the distance x from the Outer Helmholtz Plane of the double layer and on time t, and D is the diffusion coefficient. If we consider a process under the influence of an alternating current of frequency ω such that:

$$i(x,t) = I(x)e^{j\omega t} \qquad \{1.25\}$$

and further, if we assume that (a) at x = 0 the rate of diffusion of ions equals the rate at which ions are used up in the exchange current process, that is:

$$D\left(\frac{\partial c(x,t)}{\partial x}\right)_{x=0} = -\frac{i(x,t)}{zF} \qquad \{1.26\}$$

where z = ion valency and F is Faraday's constant (96,489 coulombs), the charge on one mole of ions, (b) the current gradient at the double layer surface is proportional to the time rate of change of the ion concentration at the plane or:

$$\left(\frac{\partial i}{\partial x}\right)_{x=0} = -zF \frac{\partial c(x,t)}{\partial t} \qquad \{1.27\}$$

and finally (c) as a result of the applied current there

will be a harmonic variation in the ionic concentration at the double layer surface such that:

$$c(x,t) = C(x)e^{j\omega t} \qquad \{1.28\}$$

By substitution of Eq. {1.25} and Eq. {1.28} into Eq. {1.26} and Eq. {1.27}, we may convert to phasor notation:

$$\frac{dC(x)}{dx} = -\frac{1}{zFD} I(x) \qquad \{1.29\}$$

$$\frac{dI(x)}{dx} = -j\omega zFC(x) \qquad \{1.30\}$$

To obtain an equation in C(x) only, differentiate Eq. {1.29} with respect to x and substitute for $\frac{dI(x)}{dx}$ from Eq. {1.30}, then:

$$\frac{d^2C(x)}{dx^2} - j\frac{\omega}{D} C(x) = 0 \qquad \{1.31\}$$

The general solution of Eq. {1.31} is:

$$C(x) = Ae^{-\left[j\frac{\omega}{D}\right]^{\frac{1}{2}}x} + Be^{\left[j\frac{\omega}{D}\right]^{\frac{1}{2}}x}$$

$$= Ae^{-(1+j)\left[\frac{\omega}{2D}\right]^{\frac{1}{2}}x} + Be^{(1+j)\left[\frac{\omega}{2D}\right]^{\frac{1}{2}}x} \qquad \{1.32\}$$

where A and B are constants. The second term on the right is physically impossible as it causes C(x) to become very large with distance, so we may conclude that B = 0. Thus, Eq. {1.32} becomes:

$$C(x) = C(0)e^{-(1+j)\left[\frac{\omega}{2D}\right]^{\frac{1}{2}}x} \qquad \{1.33\}$$

where C(0), the concentration at the double layer, replaces A. Because of the concentration gradient of ions near the double layer surface a concentration overpotential will exist. This overpotential is defined as the difference

between the electrode potential measured while ions flow across the interface and the equilibrium potential of the electrode. The concentration overpotential may be obtained via the Nernst Equation (Bockris and Reddy, 1970; Bockris; 1954; Bockris, 1951) as:

$$E(x) = \frac{RT}{zF} \ln \left(1 + \frac{C(x)}{C_s}\right) \qquad \{1.34\}$$

where C_s is the concentration of ions in the bulk solution. A power series expansion of Eq. {1.34} yields a linearized version based on the condition that $C(x) << C_s$. This is the case if the excitation voltage is kept low enough, thus:

$$E(x) = \frac{RT}{zF} \frac{C(x)}{C_s} \qquad \{1.35\}$$

Combination of Eq. {1.33} and Eq. {1.35} gives:

$$E(x) = \frac{RT}{zF} \frac{C(0)}{C_s} e^{-(1+j)\left[\frac{\omega}{2D}\right]^{\frac{1}{2}} x} \qquad \{1.36\}$$

Differentiating Eq. {1.33} with respect to x and substituting the result into Eq. {1.29} yields:

$$I(x) = (1+j)\, zF \left[\frac{D\omega}{2}\right]^{\frac{1}{2}} C(0) e^{-(1+j)\left[\frac{\omega}{2D}\right]^{\frac{1}{2}} x} \qquad \{1.37\}$$

From Eqs. {1.36} and {1.37} an expression for the diffusion zone impedance is obtained:

$$Z = \frac{V}{I}$$

so that:

$$Z = (1-j) \frac{RT}{(zF)^2} \frac{1}{C_s} \left[\frac{1}{2D\omega}\right]^{\frac{1}{2}} \qquad \{1.38\}$$

or defining,

$$\sigma = \frac{RT}{(zF)^2} \frac{1}{C_s} \left[\frac{1}{2D}\right]^{\frac{1}{2}}$$

Eq. {1.38} becomes:

$$Z = (1-j)\ \sigma\omega^{-\frac{1}{2}} \qquad \{1.39\}$$

Hence we see that the diffusion zone impedance may be pictured to behave as a frequency dependent diffusion resistance, $R_d = \sigma\omega^{-\frac{1}{2}}$ and a capacitive reactance, $X_d = \sigma\omega^{-\frac{1}{2}}$. This impedance is commonly known as the Warburg Impedance and will be given the notation Z_w.

At this point it is appropriate to examine the frequency dependence of the diffusion layer thickness, δ, in view of Eq. {1.26}. Extrapolating the linear part of the concentration versus distance curve and extending it to intersect with the bulk solution concentration, C_s, the diffusion layer thickness δ may be defined (Bockris and Reddy, 1970):

$$\frac{i}{zF} = -D\ \frac{C(0)}{\delta(t)} \qquad \{1.40\}$$

$$\text{where,} \quad \delta(t) = [\pi Dt]^{\frac{1}{2}} \qquad \{1.41\}$$

$$\text{or,} \quad \delta(\omega) = \left[\frac{2D}{\omega}\right]^{\frac{1}{2}} \qquad \{1.42\}$$

We see that as the frequency decreases, the diffusion layer thickness must increase. Eventually there comes a point where one dimensional motion of diffusion ions is disrupted by convective electrolyte flow attempting to compensate density changes and the diffusion zone

can no longer exist beyond some maximum distance (Bockris and Reddy, 1970). The frequency at which this transition begins to occur will depend upon the diffusion layer thickness in comparison with electrode diameter d. Eq. (1.40) is valid only if:

$$\delta < d$$

$$\text{or,} \quad \left[\frac{2D}{\omega}\right]^{\frac{1}{2}} < d$$

$$\text{giving,} \quad \omega > \frac{2D}{d^2} \qquad (1.43)$$

As mentioned earlier, the Warburg Impedance is a distributed parameter system. The voltage drop along the conductive path towards the bulk solution ($x = \infty$) is in phase with the current due to a resistance R ohms per unit distance. Associated with the electric field and charge distribution is a capacitance C farads per unit length between the conductive path and the bulk solution. The system is equivalent to a transmission line where one of the conductors has uniform resistance R per unit length and is coupled by a capacitance C per unit length to a second conductor having negligible resistance. Fig. 1.6 shows a section of such a transmission line.

If we consider a differential length dz of the line, the voltage change across it is:

$$\frac{\partial V}{\partial z}\, dz = -RdzI$$

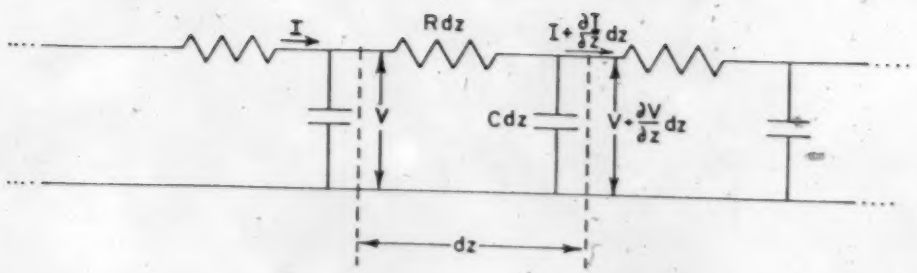

Figure 1.6 Transmission line equivalent circuit of the Warburg Impedance.

giving, $$\frac{\partial V}{\partial z} = -RI \qquad \{1.44\}$$

Also at any instant the decrease in current is the current that is shunted by the distributed capacity, or:

$$\frac{\partial I}{\partial z}\, dz = -C dx \frac{\partial V}{\partial t}$$

giving, $$\frac{\partial I}{\partial z} = -C \frac{\partial V}{\partial t} \qquad \{1.45\}$$

Differentiating Eq. {1.44} with respect to z and substituting Eq. {1.45} into the result for $\frac{\partial I}{\partial z}$ gives:

$$\frac{\partial V}{\partial t} = \frac{1}{RC} \frac{\partial^2 V}{\partial z^2} \qquad \{1.46\}$$

Eqs. {1.44}, {1.45} and {1.46} are clearly analogous to the linear diffusion Eqs. {1.26}, {1.27} and {1.24} respectively, and by the same methods used to solve the latter equations, the impedance of the transmission line results as:

$$Z = (1-j) \left[\frac{R}{2\omega C}\right]^{\frac{1}{2}} \qquad \{1.47\}$$

where by comparison with Eq. {1.38}, $\sigma \equiv \left[\frac{R}{2C}\right]^{\frac{1}{2}}$

All of the electrode impedance components which have been piecewise described to this point may now be lumped into a net equivalent circuit as shown in Fig. 1.7. Due to the frequency dependence of some elements and the dominating magnitudes of others, it is not necessary to carry out a lumped network analysis unless specific electrode information is desired (eg. Pollak, 1974). The electrode frequency response behavior may be predicted by separate consideration of the elements at low, mid range

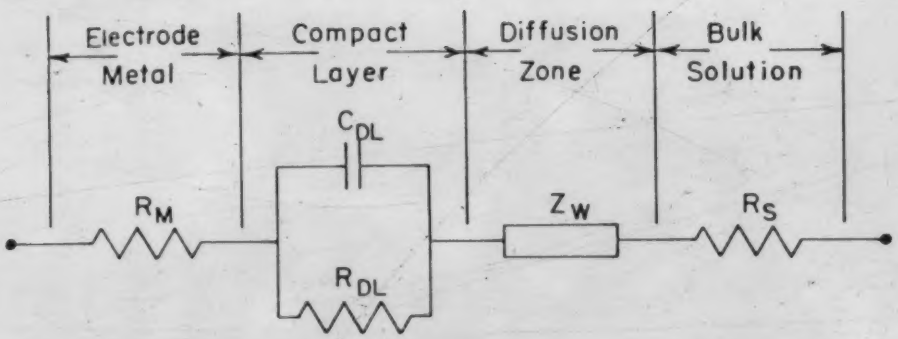

Figure 1.7 Equivalent circuit of electrode impedance.

and high frequencies.

In the mid-frequency region the electrode impedance will be chiefly controlled by the Warburg Impedance, Z_W. A 10 dB per decade roll-off of the impedance magnitude may be expected until finally, at some higher frequency, the impedance of the diffuse layer will be negligible in comparison to the spreading bulk solution resistance, R_S. Thus, at high frequencies the electrode impedance can be anticipated to level off at some value, R_S.

At very low frequencies natural convection of the bulk solution limits the increase in diffusion layer thickness with decreasing excitation frequency (Bockris and Reddy, 1970). For this reason the Warburg Impedance will be unable to continue its 10 dB per decade rise in magnitude but instead will be forced to level off at some constant value with further decreases in frequency.

Electrode surface roughness also affects the electrode impedance at low solution concentrations. Work along this line has been done extensively by de Levie (de Levie, 1965; de Levie, 1967). Warburg impedance behavior has been shown theoretically to exist in microscopic pores perpendicular to the smooth metal surface. By decreasing the depth of the pores, a porous electrode may approximate a rough electrode and the results determined for porous electrodes may be crudely applied. Development in this area however, has been scarce and primarily qualitative. Evidence for the surface roughness effect stems from

measurements of frequency dependent double layer capacitance from solidpolarizable electrodes not carrying a faradaic current (de Levie, PP. 371 to 389, 1967). It has been observed that the frequency dependence decreased markedly as the solid electrode is heated to its melting point. Whatever the resulting behavior may be, it is clear that surface roughness must affect electrode impedance in some manner. A uniform current density cannot exist over a rough surface as current flow would tend to favor protruding areas over recessed areas. Inhomogeneity of the electric field and the diffusion flow must also exist.

Adsorption of neutral or unionized substances onto the electrode surface has also been shown to produce a frequency dependence of the double layer capacitance (Parsons, 1961). The cause is attributed to variations in the double layer charge, affected by the presences of neutral substances and their slow rate of adsorption, compared to ions, while following alternating potential variations. The resulting impedance is much more complicated than the Warburg Impedance, but terms containing $\left[\frac{\omega}{2D}\right]^{\frac{1}{2}}$ are present in both numerators and denominators of the impedance expression.

CHAPTER 2

MEASUREMENT OF THE REGENERATION ELECTRODE IMPEDANCE

We have seen in Chapter 1 that the electrode interface significantly complicates the impedance pathway of the signal source. When attempting to obtain experimental measurement of this electrode impedance, the magnitude of the test signal amplitude is of particular importance. In the case of the regeneration electrodes, very small signal amplitudes are expected (in the order of 50 microvolts), which means it will be operating well within its linear impedance region. Consequently, when performing impedance measurements, the test voltage applied to the electrode must be maintained small enough to approximate this same linear behavior.

2.1 The Measuring Set-Up

The measurement of the regeneration electrode impedance evolved into two phases. In the initial phase it was desirable to gain some preliminary knowledge of what the impedances of the recently devised electrodes would in fact be. Since different fabrication techniques were being tested, it was also necessary to detect any gross differences between electrode types and to collect pre-implant data, so that the best leads could be selected after regeneration of nerve fibres has occurred. Thus, initially, the impedance measured at 1 k Hz, the commonly accepted mean frequency of extracellular spike activity, was adequate to specify the

electrode properties.

In order to specify amplifier input requirements for the regeneration electrodes, it was advantageous to seek impedance measurements over the recording bandwidth of nerve spike activity from 100 Hz to 10 kHz. In some cases the measurement bandwidth was extended to gain a complete picture of the electrode properties.

The set-up used for the impedance measurements is shown schematically in Fig. 2.1. The electrode was plaxed in a glass beaker filled with amphibian ringer solution as the electrolyte. A large bare silver wire was used as the second or ground electrode. Since the surface area exposed to the electrolyte from this electrode was large, its impedance was considered negligible in comparison. Before measurements were made, the beaker and contents were placed in an ultrasonic cleaner to vibrate the tiny air bubbles out of the regeneration electrode holes. They were then left alone for a minimum of three hours to allow for electrochemical stabilization of the electrode interface.

Resistors R_1 and R_2 functioned to reduce the amplitude of the constant voltage oscillator to a level small enough to operate the electrode in its linear region Maximum peak amplitude applied across the electrode during measurements was 10 mv. With switches S_2 closed and S_1 open, the variable calibrating resistor R_c was adjusted until the voltage amplitude monitored across the electrode

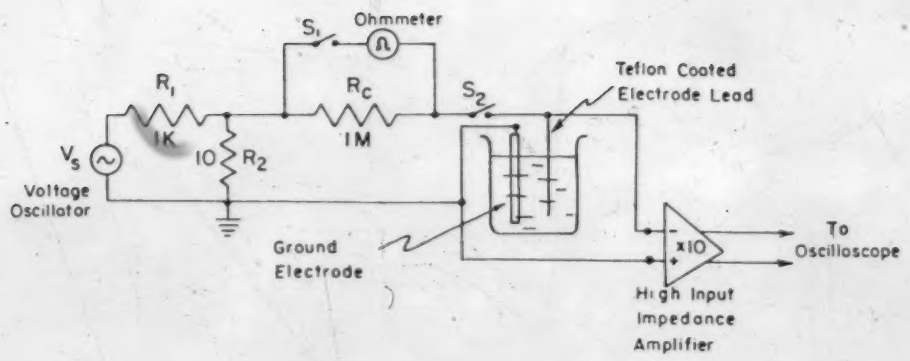

Figure 2.1 Schematic diagram of set-up used to measure the electrode impedance.

was half that of the source voltage, V_s. Switch S_2 was then opened and S_1 closed and the value of R_c measured with the ohmmeter. This value of R_c was then used as the approximate (see Appendix I) value of the magnitude of the electrode impedance.

The small value of the source signal voltage caused slight noise problems at very low frequencies, especially when electrode impedances were high. Shielding the beaker with a grounded sheet metal cylinder helped to reduce this problem. Shunt capacitance created problems only at frequencies above 10 kHz, but again this problem was not significant unless the electrode impedances were very high.

2.2 Measured Results

Single frequency impedance measurements at 1 kHz were made on 15 regeneration electrode units. In total, impedance data from 117 electrode leads was collected. Leads disregarded were those with impedances too low or less than 25 K ohms, and those with impedances too large or much greater than 1 M ohm. A wide variation in electrode impedances was expected due to fabrication tolerance. For example, a drilled hole may not meet precisely on center with a silver wire but may nick a corner, thus causing the impedance to be higher than normal. The mean average impedance of the 117 electrode leads tested was 122 K ohms.

Fig. 2.2 shows the impedance-frequency response characteristic of a single electrode lead. A 10 dB per

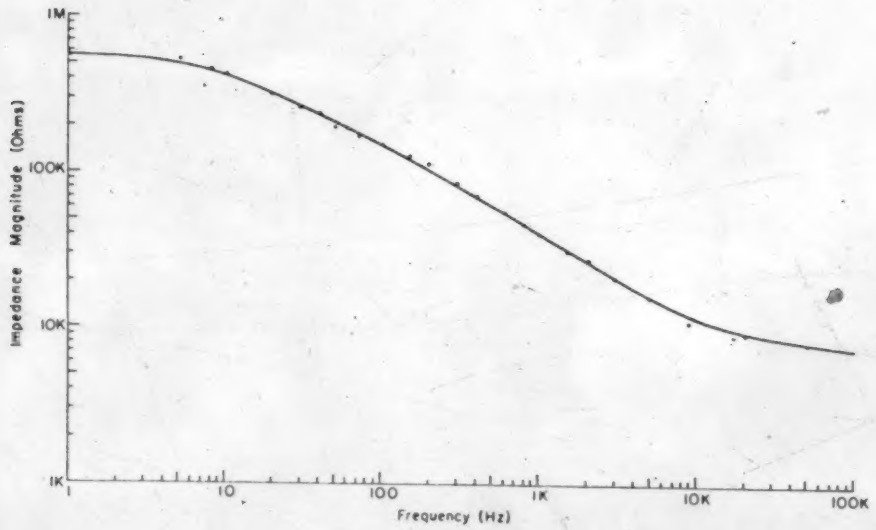

Figure 2.2 Impedance characteristic of a single REU lead.

decade decrease in the mid-frequency region clearly demonstrates the presence of the Warburg Impedance due to the interphase diffusion layer, as discussed in Chapter 1. At frequencies of about 10 kHz the curve begins to level off, indicating a bulk saline resistance near 8 K ohms which may be considered the resistance of the electrode channel. This value is considerably below the theoretical value of 30 K ohms indicated in section 1.2 and is probably a result of the following: A wire embedded off-center in the epoxy slab will sit too close to one side of the hole, thus reducing the effective channel resistance. Secondly, surface roughness and smearing of the silver wire from drilling could be causing a marked increase in the electrode surface area in contact with the saline. This second reason can be substantiated by comparing Fig. 2.2 to Fig. 2.3 which shows the impedance characteristic of a single 76 micron teflon coated silver wire with its cross-section only exposed to saline. The 40 K ohm value of bulk saline resistance obtained from Fig. 2.3 is about 5 times higher, indicating a significant decrease in electrode surface area.

Impedance characteristics of 6 leads from a single regeneration unit are shown in Fig. 2.4, illustrating the lead-to-lead variations that are encountered. The 1 kHz impedances vary from 68 K ohm to 15 K ohm. An average plot taken from measurements from 6 leads of another electrode unit is indicated in Fig. 2.5. Here the average 1 kHz impedance is 45 K ohms.

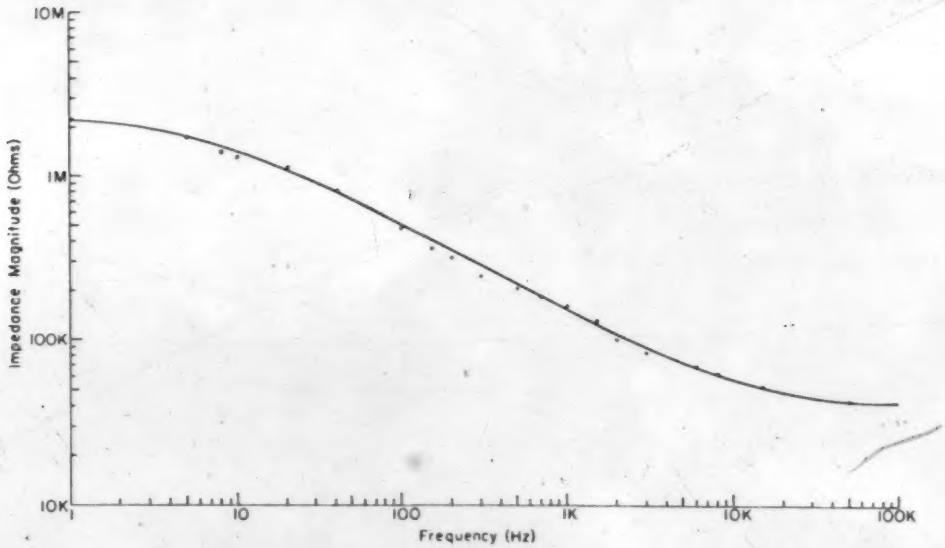

Figure 2.3 Impedance characteristic of a single 76 micron teflon coated silver wire.

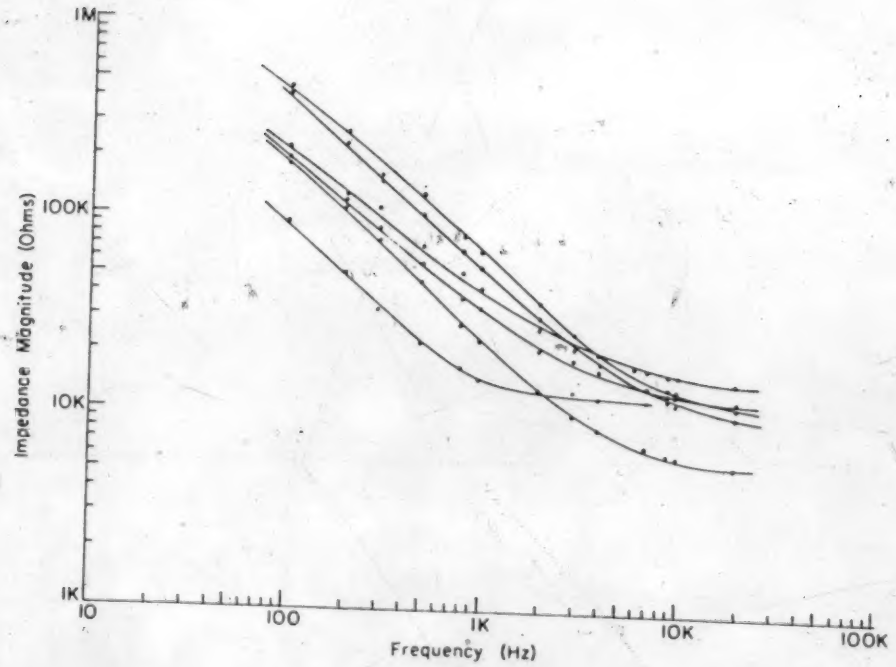

Figure 2.4 Impedance characteristics of 6 REU leads.

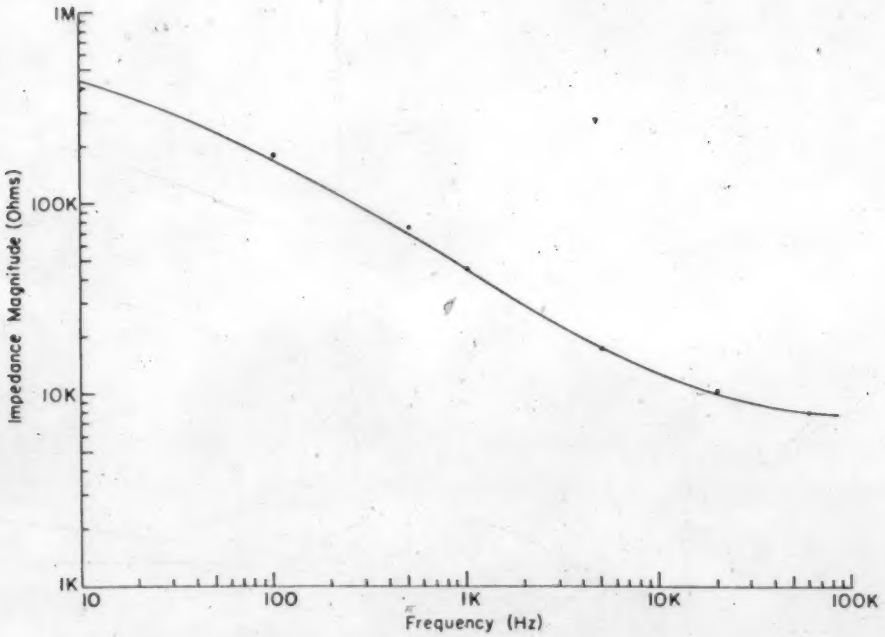

Figure 2.5 Average impedance characteristics of 6 REU leads.

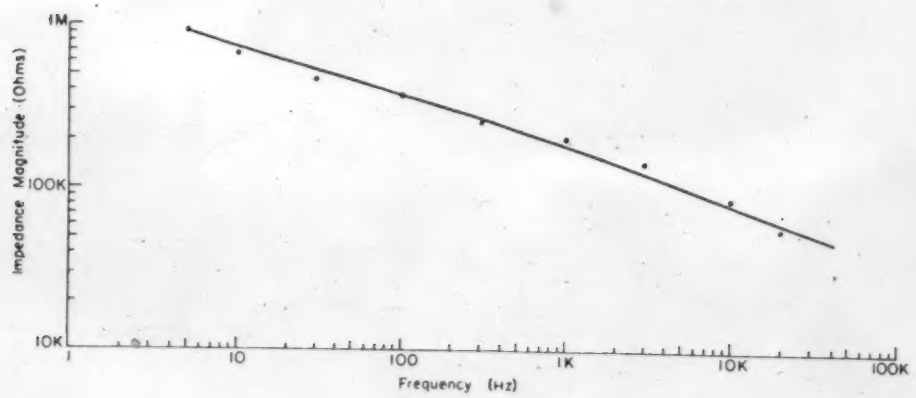

Figure 2.6 Impedance characteristic of a pair of implanted REU leads.

Impedance measurements of implanted electrodes have not been routinely tested so far, due to apprehension that the test currents could seriously disrupt regenerating nerve fibres. Some measurements were made on an unsuccessful implant still in-situ. Eighteen lead-to-lead measurements at 1 kHz gave an average impedance of 345 K ohms or an average single lead value of about 170 K ohms. Response from 10 Hz to 10 kHz of one pair of these leads is shown in Fig. 2.6.

2.3 Implications for the Recording Amplifier

A detailed description of the implantation of the electrode is presented in Mannard, Stein and Charles, 1974. A summary of this description is given here.

The object nerve is cut about three-quarters through the cross section and a 3 mm length of polyethylene tubing, prepared with a notch to accept the regeneration electrode unit (REU), is placed around the nerve to form a cuff around the cut section. Next the REU is placed into the notch in such a manner as to allow the nerve fibres to tunnel through the holes during regeneration. After it is in place, the REU is sutured tightly to the cuff. Leads from the electrode are connected to a multi-pin socket imbedded in a biologically inert skin button which is located at some convenient access point on the body surface. An x-ray photograph of one implant in the leg of a cat is shown in Fig. 2.7.

Tentative arrangements for recording signals from

Figure 2.7 X-ray photograph of implant regeneration electrode unit in the leg of a cat.

the REUs involve connecting amplifier channels directly to the skin button socket. Running coaxial cable from the socket to the amplifiers is an undesirable situation because of cable shunt capacitance, electrostatic noise induced by mechanical vibration, and cable bulk. Consequently, it would be far more preferable to place the input transistors of a recording amplifier directly at the skin socket and obtain downward impedance transformation of the source signal so that coaxial cables will no longer be necessary. With this arrangement the only matter of concern will be shunt capacitance present in the electrodes and leads.

Since the electrode is simply the tip of the lead wire, attention need only be given to the capacitance between the lead core wire and the surrounding electrolyte fluid. The capacitance across insulation of relative dielectric constant ϵ_r, separating the core wire of diameter, d, and a concentric outer conductor of diameter D which of course is the electrolyte bath, can be calculated from (Robinson, 1968):

$$C_s = \frac{0.245\ \epsilon_r}{\log_{10}\left[\frac{D}{d}\right]} \quad \text{pF/cm}$$

Using $\epsilon_r = 2.1$ for teflon

$D = 0.0045$ in. $= 1.143 \times 10^{-2}$ cm

$d = 0.0030$ in. $= 7.62 \times 10^{-3}$ cm

gives a value of 2.92 pF/cm. Since maximum lead lengths of 10 cm are expected, the maximum shunt capacitance per lead

will be approximately 30 pF.

An equivalent input network of a single electrode amplifier connection is represented in Fig. 2.8. For simplicity, the electrode impedance is treated as an equivalent series combination of conductance R_E and reactance $-X_E$, and the shunt capacitance as a lumped value of C_S. At a given frequency f the input voltage V_i seen by an amplifier of input resistance R_i will be:

$$V_i = \left[\frac{R_i}{R_i + R_E + 2\pi f X_E R_i C_S + j(X_E + 2\pi f R_i R_E C_S)} \right] V_S \qquad \{2.1\}$$

Therefore, to assure maximum input voltage to the amplifier the bracketed portion of Eq. {2.1} should take on values close to 1.

If the amplifier is chosen so that its input impedance is very much greater than the electrode impedance or $R_i >> R_E$ and $R_i >> X_E$ than Eq. {2.1} may be approximated as:

$$\frac{V_i}{V_S} = \frac{1}{1 + 2\pi f X_E C_S + j 2\pi f R_E C_S}$$

$$\text{or} \quad \left| \frac{V_i}{V_S} \right| = \frac{1}{\left[(1 + 2\pi f X_E C_S)^2 + (2\pi f R_E C_S)^2 \right]^{\frac{1}{2}}} \qquad \{2.2\}$$

A practical estimate of this value at 1 kHz can be made. Since values in the order of 100 K ohms can be expected for X_E and R_E and, using a maximum of 30 pF of predicted shunt capacitance, Eq. {2.2} is evaluated as:

$$\left| \frac{V_i}{V_S} \right| = \left[\{1 + 2\pi (10^3)(10^5)(3 \times 10^{-11})\}^2 + \{2\pi (10^3)(10^5)(3 \times 10^{-11})\}^2 \right]^{-\frac{1}{2}}$$

$$= 0.98$$

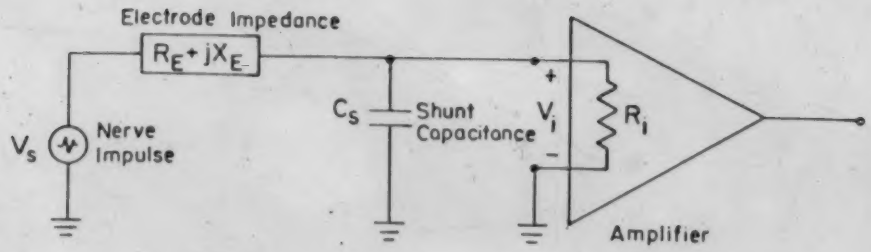

Figure 2.8 Amplifier-source equivalent input circuit.

Thermal noise will also be added to the source voltage due to the conductive mechanisms in the recording electrode. The rms noise voltage E_t produced from an electrode resistance in the order of 100 K ohms can be obtained from the Nyquist relation:

$$E_t = \sqrt{4KTR\Delta f}$$

where R = the electrode resistance

$4kT = 1.61 \times 10^{-20}$ at 290 ^{o} K

and Δf = noise bandwidth in Hz

Since a 3dB recording bandwidth of 5 kHz is planned the corresponding noise voltage produced will be:

$$E_t = \left[(1.61\text{x}10^{-20})(10^5)(\tfrac{\pi}{2}\text{x}5\text{x}10^3)\right]^{\frac{1}{2}}$$

$$E_t = 3.6\ \mu \text{ volts}$$

Nerve signals of about 10 times this value are expected, giving an input signal to noise ratio of 20 dB. If the recording amplifier used were to have a noise figure of 3 dB the output signal will be increased to 20 times the output noise level. It would be desirable therfore to use an anplifier with a noise figure of less than 3 dB.

CHAPTER 3

REGENERATION ELECTRODE AMPLIFIER

3.1 General

The REU impedance measurements discussed in Chapter 2 are useful in specifying the properties of the recording amplifier that will be required for this device. An average impedance magnitude of 100 K ohms indicates that a high input impedance amplifier is necessary. Since shunt capacitance is not significantly present in the electrode, the use of input capacity neutralization will not be required. The extremely small signal level and high noise level of the source electrode dictate the necessity of a very low-noise amplifier.

In section 2.3 it was mentioned that due to limited space conditions in the vicinity of the electrode skin socket, it would be advantageous to place only the input transistor of the amplifier onto the skin socket. This would allow connection via long flexible wires to be made to the actual amplifier body, placed at some convenient distance away from the recording site. An amplification method developed by Bergveld, 1968, offers a satisfactory means of achieving this set-up, while also satisfying the other amplifier requirements stated above.

3.2 Amplification Method

Placing a field effect transistor at the test sight, and having the drain and source of the device make

connection via long leads to low-ohmic points (in the order of 100 ohms) enables relatively interference free signal transmission to be achieved. A set of conditions must be satisfied so that an interference noise voltage commonly introduced to both leads is not allowed to influence the drain current of the FET, (Bergveld, 1968). These conditions are that, (1) the low ohmic drain connection must equal the low ohmic source connection, and (2) the FET must be biased such that its amplification factor μ takes on a value $\mu<1$. This second condition requires the FET to be biased in the "ohmic" region where it will behave as a voltage variable resistor (VVR). The circuit of Fig. 3.1 shows the set-up used to achieve the proper FET bias and balanced low ohmic coupling.

3.3 D.C. Analysis

The important factors that govern the transistor current bias levels entail the following:

1. V_{DS} of the FET should be such that it will operate in the "ohmic" region. Characteristic I_D vs. V_{DS} curves for several 2N3819 FETs were tested on a curve tracer. The devices with the lowest knee voltage (500 mv) were selected for use, as these required low bias voltage levels and hence fewer biasing diodes. For best linear operation it is best to choose an operating voltage such that $V_{DS}<\frac{1}{2}V_{knee}$, therefore V_{DS} = 200 mv. was used.
2. V_{GS} of the FET should be such that the device will operate in a region where g_m is substantially large without

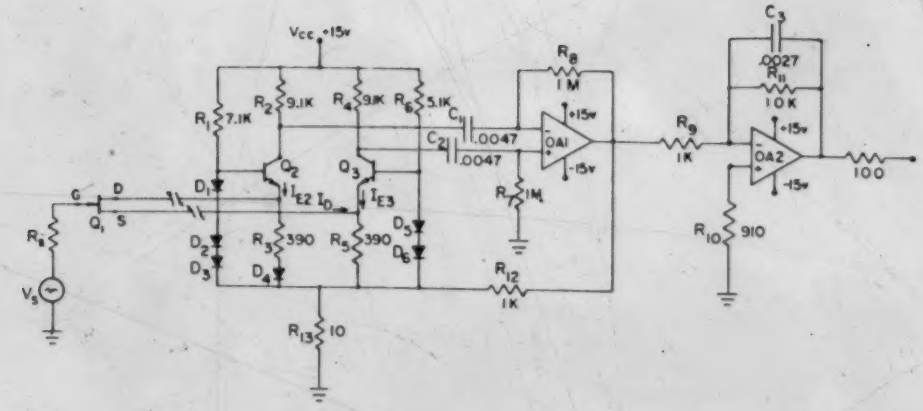

Figure 3.1 Amplifier circuit diagram:

$Q_2 = Q_3$: Fairchild 2N3117 bipolar low noise transistor

Q_1: Texas Instruments 2N3819 field effect transistor

D_1: Elcom ED4 germanium diode

$D_2=D_3=D_4=D_5=D_6$: Elcom ED21 silicon diode

OA1 = OA2: RCA6741T operational amplifier (low noise)

demanding extremely large drain current levels. From the curve tracer characteristics a V_{GS} value of 600 mv. was found to be satisfactory. At this operating point g_m had a value of 1.2 mmho and I_D was about 460 microamps.

3. The collector current levels of the bipolar transistors Q_2 and Q_3 should be such that the devices are working in their lowest noise region. For reasons to be discussed later in section 3.6 based on data supplied by the manufacturer, the 2N3117 transistor was selected on the basis that it achieved low noise operation when biased in the neighborhood of 1mA. Many transistors are available that can obtain low noise operation at significantly lower current levels. However in this application larger current levels are necessary because of current demands of the FET.

Giving consideration to the above factors the d.c. analysis of the input stage is as follows. Since both Q_2 and Q_3 must draw the same current of 1mA:

$$\text{Current through } R_3 = I_{E2} - I_D$$

$$= 1\text{mA} - 0.5\text{ mA}$$

$$I_{R3} = 0.5\text{ mA}$$

$$\text{Current through } R_5 = I_{E3} + I_D$$

$$= 1\text{mA} + 0.5\text{ mA}$$

$$I_{R5} = 1.5\text{ mA}$$

The voltage at the emitter of Q_3 is determined by V_{GS} of the FET since $V_{E3} = V_{GS} = 0.6$ v. Hence the value of R_5 should be:

$$R_5 = \frac{V_{E3}}{I_{R5}} = 400\ \Omega$$

In section 3.2 it was cited that the drain and source of the FET must both terminate on equal low ohmic connections. Therefore R_3 must also take on a value of 400 ohms. A required current level of 0.5 mA through R_3 means a corresponding 0.2 v. drop across it. This voltage must be supplemented by the 0.6 v. forward bias voltage of a silicon diode placed in series with R_3 to create the necessary 0.8 v. level at the emitter of Q_2, since:

$$V_{E2} = V_{E3} + V_{DS} = 0.6v + 0.2v = 0.8v$$

The required voltage at the base of Q_2 must then be:

$$V_{B2} = V_{BE2} + V_{E2} = 0.6v + 0.8v = 1.4v$$

which suggest the use of two 0.6 v. silicon diodes and one 0.2 v. germanium diode. The resistance R_1 is chosen to set the proper current levels through D_1, D_2 and D_3 to attain this voltage. Similarly, the voltage at the base of Q_3 must be:

$$V_{B3} = V_{BE2} + V_{E3} = 0.6v + 0.6v = 1.2v$$

which suggest the use of two 0.6 v. silicon diodes.

The circuit of Fig. 3.1 was constructed using the closest resistor values available. Measured d.c. values from the actual circuit were as follows:

I_{C2} = 1.17 mA. I_{C3} = 1.01 mA.

I_{R3} = 0.72 mA. I_{R5} = 1.46 mA.

I_D = 0.45 mA. V_{DS} = 0.22 v.

Using the latter two measurements for the FET, a working

value for the drain to source resistance is obtained:

$$R_d = \frac{V_{DS}}{I_D} = 490\ \Omega$$

3.4 A.C. Analysis

1. Representing the FET: Since the FET is operated as a voltage variable resistor, changes in V_{GS} will regulate drain resistance and hence drain current. The drain to source voltage V_{DS} is maintained at a constant value by the circuit regulating diodes D_1 through D_6, and therfore the FET operation may be specified in terms of its trans-conductance g_m, as illustrated in Fig. 3.2:

$$g_m \equiv \left.\frac{\partial i_D}{\partial v_{GS}}\right|_{V_{DS} = \text{const.}} \qquad \{3.1\}$$

As discussed in the previous section, the FETs used operated with a constant V_{DS} of 220 mv. and V_{GS} of 640 mv. According to analysis of the curve tracer display of the device I_D vs. V_{DS} characteristics, a value of 1.2×10^{-3} mho for g_m was obtained.

2. Voltage gain at the FET drain and source: The output at the FET drain and source can be determined by analysis of the circuits of Fig. 3.3(a) and (b). Fig. 3.3(b) shows the FET drain to source pathway represented by a current generator $g_m V_{gs}$ in parallel with the drain resistance r_d. The resistance, R_i, is the equivalent input resistance of the common base stages of transistors Q_2 and Q_3. Replacing these transistors with their low frequency approximate hybrid model (Millman and Halkais, 1972, Section 8-13) the

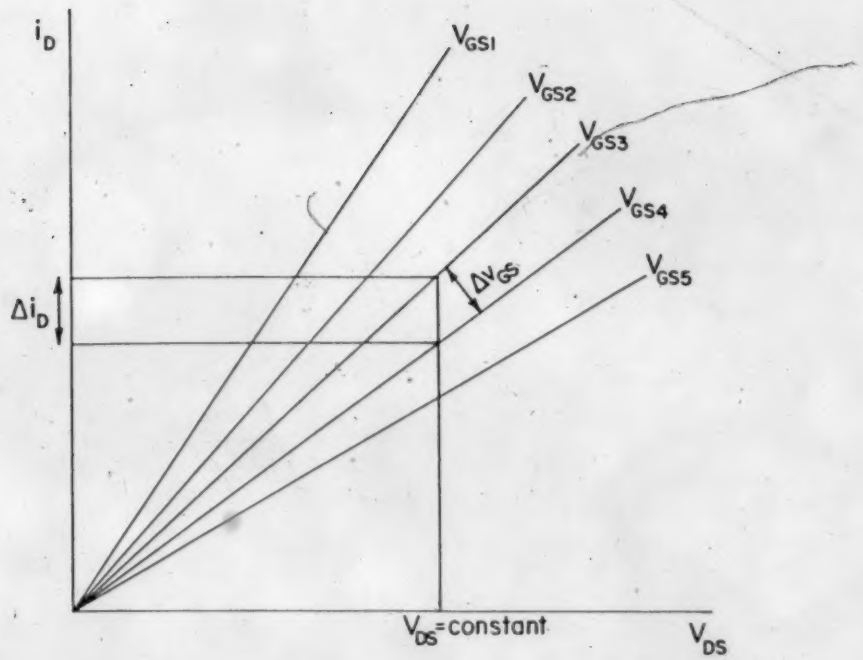

Figure 3.2 FET transconductance in the "ohmic" region:

$$g_m \simeq \left.\frac{\Delta i_D}{\Delta v_{GS}}\right|_{V_{DS} = \text{const.}}$$

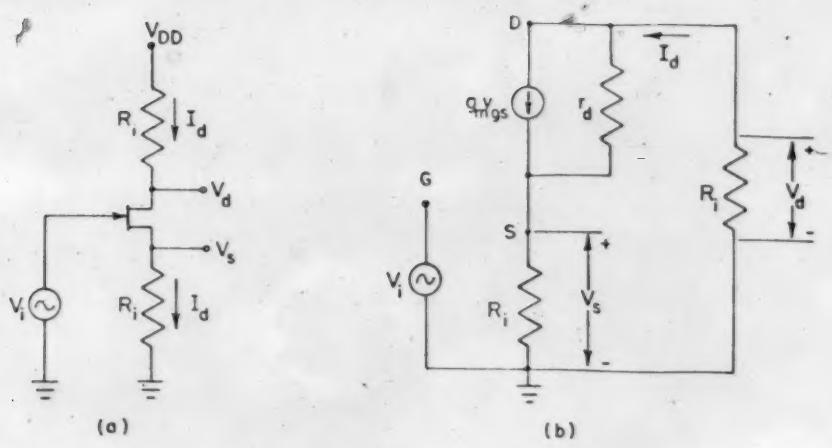

Figure 3.3 (a) FET represented in-circuit.
(b) The small signal equivalent circuit.

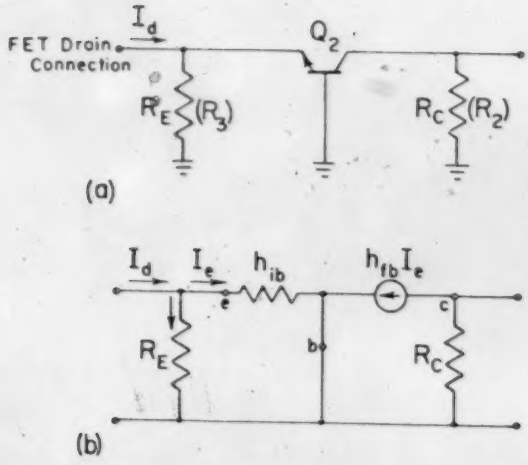

Figure 3.4 (a) A.C. pathway of transistor Q_2 illustrating common base configuration.
(b) The low frequency approximate hybrid equivalent circuit.

Note: The same circuits would also apply to transistor Q_3.

equivalent circuit of Fig. 3.4 is obtained. Analysis of this circuit gives:

$$R_i = \frac{V_d}{I_d}$$

$$\text{or,} \quad R_i = \frac{h_{ib} R_E}{h_{ib} + R_E} \qquad \{3.2\}$$

Substituting 390 ohms for the value of R_E and 27 ohms for the h_{ib} value of a 2N3117 transistor gives a value of 25 ohms for R_i.

Applying K.V.L. to the drain circuit of Fig. 3.3 (b) yields:

$$I_d R_i + (I_d - g_m V_{GS}) r_d + I_d R_i = 0 \qquad \{3.3\}$$

The voltage from G to S is given by:

$$V_{gs} = V_i - I_d R_i \qquad \{3.4\}$$

$$\text{Since} \quad V_d = -I_d R_i, \qquad \{3.5\}$$

$$V_s = I_d R_i \qquad \{3.6\}$$

and the FET amplification factor is given by:

$$\mu = g_m r_d \qquad \{3.7\}$$

we may combine Eqs. {3.3} through {3.7} to give:

$$\frac{V_s}{V_i} = -\frac{V_d}{V_i} = \frac{\mu R_i}{r_d + (\mu+2) R_i} \qquad \{3.8\}$$

The drain-source resistance, r_d, was evalued in section 3.3 as 490 ohms. Using the value of 1.2×10^{-3} mho as measured for g_m, Eq. {3.7} yields $\mu = 0.588$. Substitution

of the proper values into Eq. {3.8} gives:

$$\frac{V_s}{V_i} = -\frac{V_d}{V_i} = 0.027 \qquad \{3.9\}$$

This result compares quite favorably with actual measured values from the circuit, which were:

$$\frac{V_d}{V_i} = -0.030 \text{ and } \frac{V_s}{V_i} = 0.026$$

The small variation is likely due to differences in h_{ib}.

3. Input stage voltage gain: Expressions for the voltage gains at the collectors of Q_2 and Q_3 may be obtained by analysis of the equivalent circuit of Fig. 3.5(b). For the FET we have:

$$I_3R_E + (I_d - g_m V_{gs})r_d + I_5R_E = 0 \qquad \{3.10\}$$

and since $$V_{gs} = V_i - I_5R_E \qquad \{3.11\}$$

and $$I_3 = I_d + I_{e1} \qquad \{3.12\}$$

$$I_5 = I_d - I_{e2}$$

Eqs. {3.10} through {3.12} may be combined to give:

$$I_d(r_d + (\mu+2)R_E) - \mu(V_i + I_{e2}R_E) + R_E(I_{e1} - I_{e2}) = 0 \qquad \{3.13\}$$

where $\mu = g_m r_d$

Noting the current division at the emitters of Q_2 and Q_3, we may write:

$$\frac{I_{e2}}{I_d} = -\frac{I_{e1}}{I_d} = \frac{R_E}{h_{ib} + R_E} \qquad \{3.14\}$$

The output voltage from Q_2 is:

$$V_{o1} = -h_{fb}R_C I_{e1} \qquad \{3.15(a)\}$$

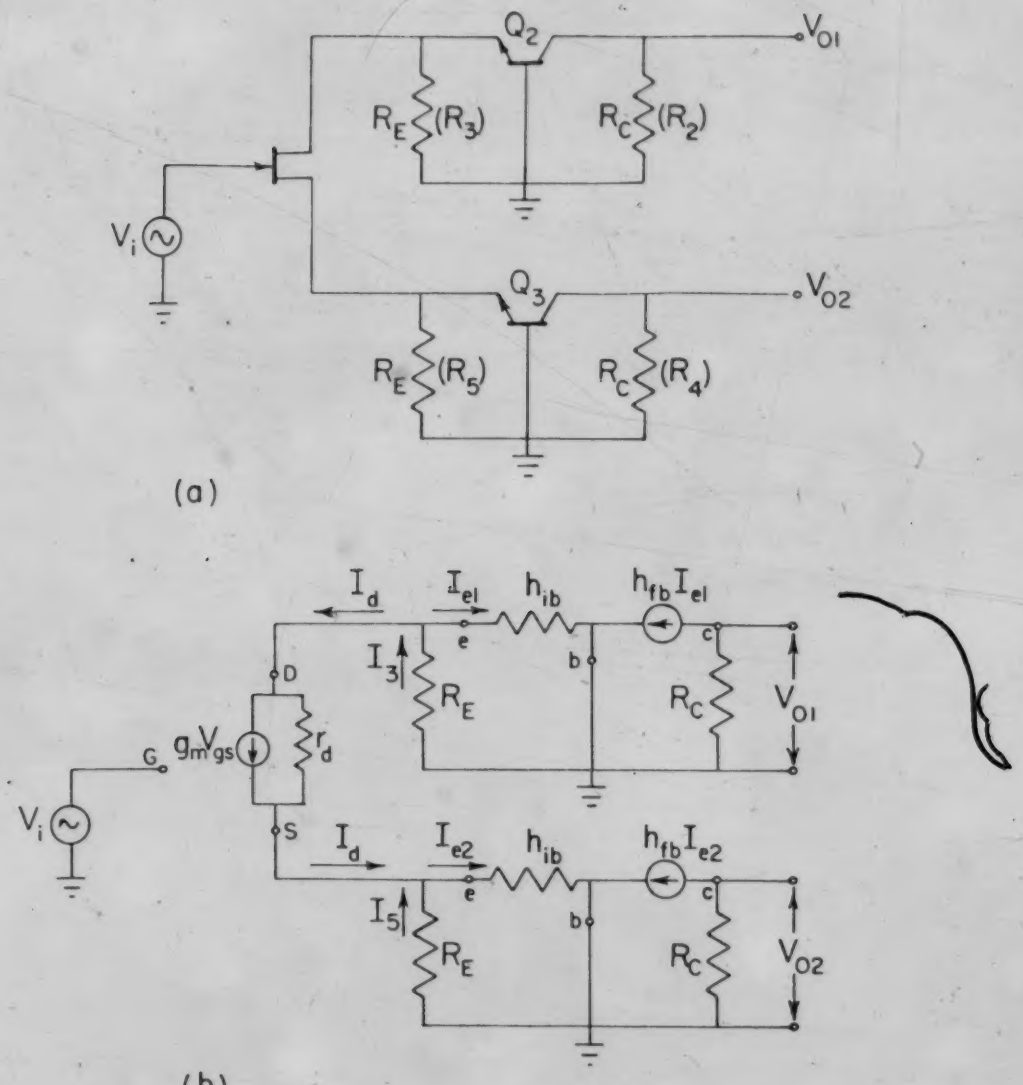

Figure 3.5 (a) A.C. pathway of amplifier input stage.
(b) Equivalent circuit of same.

and the output from Q_3 is:

$$V_{02} = -h_{fb}R_cI_{e2} \qquad \{3.15(b)\}$$

It follows from Eq. {3.14} that $I_e = I_{e1} = -I_{e2}$ and therefore $V_{01} = -V_{02}$. Eq. {3.13} may now be rewritten as:

$$I_d(r_d+(\mu+2)R_E) + I_e(\mu+2)R_E = \mu V_i \qquad \{3.16\}$$

Substituting Eq. {3.14} first and Eq. {3.15(a)} second:

$$\frac{V_{01}}{V_i} = \frac{\mu h_{fb}R_cR_E}{r_d(h_{ib}+R_E) + (\mu+2)h_{ib}R_E}$$

or

$$\frac{V_{01}}{V_i} = \frac{\mu h_{fb}R_c}{r_d(1+\frac{h_{ib}}{R_E}) + (\mu+2)h_{ib}} \qquad \{3.17\}$$

Whereupon, inserting the appropriate values, namely $\mu = 0.588$, $h_{fb} = -0.9975$, $h_{ib} = 27$ ohms, $R_E = 390$ ohms and $R_c = 9.1$ K ohms gives:

$$\frac{V_{02}}{V_i} = -\frac{V_{01}}{V_i} = 9$$

or

$$\frac{V_{02} - V_{01}}{V_i} = 18 \qquad \{3.18\}$$

Comparison to the actual measured gains of the amplifier are again good, since:

$$\frac{V_{01}}{V_i}_{\text{(measured)}} = -10 \text{ and } \frac{V_{02}}{V_i}_{\text{(measured)}} = 9$$

or

$$\frac{V_{02} - V_{01}}{V_i}_{\text{(measured)}} = 19 \qquad \{3.19\}$$

4. The op-amp stages (OA1 and OA2) and circuit feedback:

A differential a.c. amplifying stage using one op-amp (OA1) follows the bipolar common base stage as shown in Fig. 3.6. Series resistors $R_2 = R_4 = 9.1$ K ohms are the effective output resistances from the Q_2 and Q_3 stages. Since the circuit noise is random and uncorrelated, the application of negative feedback will not reduce output noise levels. The feedback resistor itself will however, inject thermal noise into the circuit. The value for the feedback resistors R_8 and R_7 of 1 M ohm therefore, is a compromising value, high enough to produce sufficient open loop gain, yet low enough to add a minimal amount of noise. Analysis of Fig. 3.6 gives the following voltage gain:

$$A_v = \frac{R_f}{R_i + \frac{1}{sC}} \qquad \{3.20\}$$

where $R_f = R_7 = R_8$ and $R_i = R_2 = R_4$. Letting $\tau = R_i C_1$, Eq. {3.20} becomes:

$$A_v = \frac{R_f}{R_i} \frac{s\tau}{1 + s\tau} \qquad \{3.21\}$$

A diagram of the input circuit including overall feedback is shown in Fig. 3.7. The feedback voltage, V_f, is produced by the voltage divider, R_{12} and R_{13}, thus the feedback factor, β, is determined as:

$$\beta = \frac{R_{13}}{R_{13} + R_{12}} \qquad \{3.22\}$$

Substituting $R_{13} = 10$ ohms and $R_{12} = 1.1$ K the value of β obtained is:

$$\beta = \frac{1}{111}$$

With the feedback loop opened, the open loop gain is:

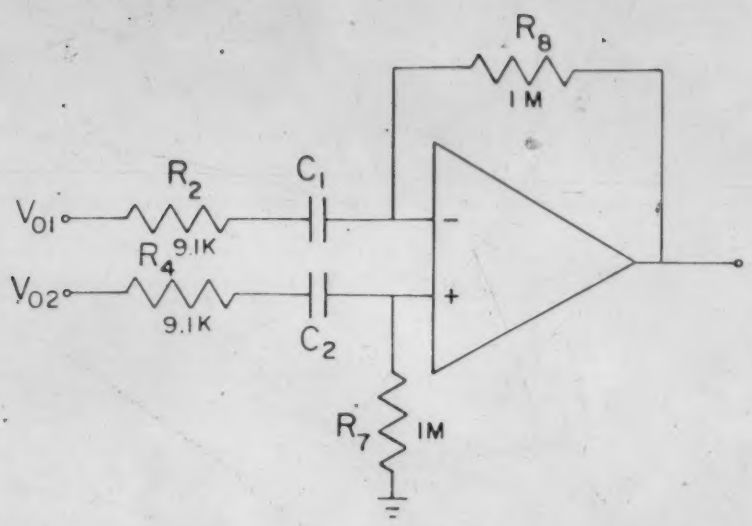

Figure 3.6 Differential a.c. coupled op-amp stage.

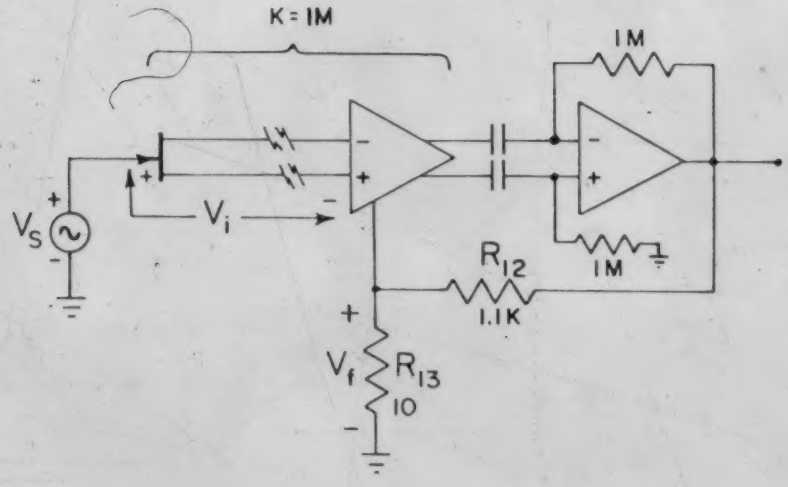

Figure 3.7 Voltage-series feedback of input circuit

$$V_i = V_s - V_f$$

$$A_v = K \frac{R_f}{R_i} \frac{s\tau}{1 + s\tau} \qquad \{3.23\}$$

where K is the amplification due to the input FET - Bipolar stage obtained in Eq. {3.19} as having a value of 19. If we let $A_o = K\frac{R_f}{R_i}$ then Eq. {3.23} may be written:

$$A_v = A_o \frac{s\tau}{1 + s\tau} \qquad \{3.24\}$$

Closing the feedback loop we may write the closed-loop gain as:

$$A_{vf} = \frac{A_v}{1 + A_v\beta}$$

$$= \frac{A_o \frac{s\tau}{1+s\tau}}{1 + \beta(A_o \frac{s\tau}{1+s\tau})}$$

and finally $$A_{vf} = \frac{A_{of}(1+A_o\beta)s\tau}{1 + (1+A_o\beta)s\tau} \qquad \{3.25\}$$

The value of the coupling capacitor $C_1 = C_2$ may be obtained using Eq. {3.25}. Since a low frequency, half-amplitude cutoff frequency of 100 Hz is proposed:

$$\left|\frac{A_{vf}}{A_{of}}\right| = \frac{|j\omega(1+A_o\beta)R_iC_1|}{|1 + j\omega(1+A_o\beta)R_iC_1|} = \frac{1}{2} \qquad \{3.26\}$$

at the cutoff frequency $\omega = 2\pi(100)$ rad/sec. Thus:

$$\frac{\omega(1+A_o\beta)R_iC_1}{\{1 + \omega^2(1+A_o\beta)^2(R_iC_1)^2\}^{\frac{1}{2}}} = \frac{1}{2}$$

or $$4\omega^2(1+A_o\beta)^2(R_iC_1)^2 = 1 + \omega^2(1+A_o\beta)^2(R_iC_1)^2$$

giving $$C_1 = \frac{1}{2\sqrt{3}\pi f(1+A_o\beta)R_i} \qquad \{3.27\}$$

Substituting f = 100 Hz, R_i = 9.1 K, $\beta = \frac{1}{111}$ and

$A_o = K \frac{R_f}{R_i} = 2088$ gives: $C_1 = 5.10 \times 10^{-9}$F.

At midband Eq. {3.25} reduces to:

$$A_{of} = \frac{A_o}{1 + \beta A_o} \qquad \{3.28\}$$

giving a closed loop midband gain of:

$$A_{of} = \frac{2088}{1 + \frac{2088}{111}}$$

or $A_{of} = 105$

An inverting amplifier is used as the final stage to provide an additional gain of 10 and high frequency roll off (Fig. 3.1). The closed loop gain is given by:

$$A_v = - \frac{R_{11}}{R_9} \frac{1}{1 + j\omega R_{11} C_3} \qquad \{3.29\}$$

For the proposed half-amplitude cutoff frequency at 10 K Hz:

$$\left| \frac{1}{1 + j\omega R_{11} C_3} \right| = \frac{1}{2}$$

or $$\left[1 + (\omega R_{11} C_3)^2\right]^{\frac{1}{2}} = 2$$

giving $$C_3 = \frac{\sqrt{3}}{2\pi f R_{11}} = \frac{\sqrt{3}}{2\pi \cdot 10^4 \cdot 10^4} \qquad \{3.30\}$$

$$C_3 = 2.76 \times 10^{-9} \text{ F}$$

3.5 Amplifier Noise Mechanisms

The three main noise mechanisms found in solid state amplifiers are referred to as thermal noise, excess or 1/f noise and shot noise (Motchenbacher and Fitchen, 1973).

Thermal Noise

Thermal noise, also known as Johnson noise and Nyquist noise, is present in all conductors as a result of the random thermal vibration of charge carriers. It is therefore the prime noise mechanism in resistors. In bipolar transistors the base spreading resistance and source resistance generate thermal noise, and in FETs, it is generated from the channel resistance. The rms noise voltage E_t of a resistance R is given by:

$$E_t = \sqrt{4KTR\Delta f} \qquad \{3.31\}$$

where $4KT = 1.61 \times 10^{-20}$ at 290^{o} K

R = pure resistance in ohms

and Δf = noise bandwidth in hertz

For circuit analysis, we may substitute a noisy resistance by a noiseless resistor of the same ohmic value in series with an rms noise voltage generator E_t.

Excess Noise or 1/f Noise

As the name implies, the spectral power density of this type of noise increases limitlessly with decreasing frequency. Carbon resistors generate excess noise when direct current is being passed. Current tends to flow unevenly through the compressed carbon granules creating "microarcs" between them. This problem can be eliminated by using tin oxide, wire wound, or metal film resistors in low noise d.c. applications. Excess noise is present in bipolar transistors as a result of base current flow

through discontinuities in the base-emitter depletion region, and in FETs from leakage gate current fluctuations. Surface impurities and dislocations are also a source of transistor excess noise. Because of its 1/f nature, excess noise need only be considered in low frequency or d.c. amplifier applications.

Shot Noise

Shot noise is present at all semiconductor junctions, and is a result of the pulsatile nature of quantum bundles of charges flowing across the junction potential barrier. In bipolar transistors, shot noise is primarily a result of base and collector currents across the base-emitter junction. In FETs shot noise is generated from the gate current flow across the gate-channel junction barrier. The rms value of shot noise current is given by:

$$I_{sh} = \sqrt{2qI_{DC}\Delta f} \qquad \{3.32\}$$

where q = electronic charge
$= 1.59 \times 10^{-19}$ coulomb
I_{DC} = direct current in amps
Δf = noise bandwidth in hertz

3.6 Active Device Noise Considerations

The FET, Q_1

FET noise voltage generated at frequencies above 1 K Hz results from the thermal noise of the channel resistance, R_d. This noise is known as van der Ziel noise and can be predicted according to:

$$E_n = \sqrt{4KTR_d\Delta f} \qquad \{3.33\}$$

The value for R_d of the 2N3819 FET was measured experimentally in section 3.3 to have a value of 490 ohms. Using this value over a 5 K Hz, 3 dB bandwidth, Eq. {3.33} gives:

$$E_n = 0.25\ \mu V$$

The channel resistance may also be approximated from:

$$R_d \simeq \frac{2}{3}\frac{1}{g_m} \qquad \{3.34\}$$

Again, from section 3.3 the value of $g_m = 1.2 \times 10^{-3}$ mho is obtained, giving:

$$R_d \simeq 550 \text{ ohms}$$

From Eq. {3.33} it is seen that van der Ziel noise is minimized by decreasing R_d or, from Eq. {3.34}, by increasing g_m; however, the degree of flexibility is limited because of the biasing conditions as per section 3.3.

At frequencies less than 1 K Hz, FET noise voltage results from excess or 1/f noise resulting from the capturing of charge carriers at the generation - recombination sites in the gate - channel depletion region. The fluctuations of charge at these sites results in a flickering gate - source noise voltage. Devices with low internal gate leakage current, I_{GSS}, will have low excess noise, however, if a high I_{GSS} value is the result of surface leakage current only, it will not affect the noise level.

Selection of the 2N3819 FET was based primarily on its ability to satisfy the circuit bias conditions, and

to obtain the largest possible value of g_m while operating in the VVR region. A maximum I_{GSS} value of 2nA, while not being the lowest available, did not appear to result in significant additional amounts of noise. The choice of a JFET over a MOSFET is more preferable, as MOSFETs have anywhere from 10 to 1000 times the excess noise level. MOSFETs are best used when source resistances are greater than 500 K ohms, which is above the average 100 K ohm regeneration electrode impedance.

The Bipolar Transistors Q_2 and Q_3

Unlike the FET, surface leakage current on a bipolar transistor chip will result in increased 1/f noise levels. For low noise applications, therefore, it is desirable to use a low leakage, surface passivated and hermetically sealed transistor.

In the midband frequency independent region of transistor operation, shot noise mechanisms will dominate, and the noise produced will be highly dependent on the value of source resistance used. The optimum operating noise factor of the transistor is obtained only when the source resistance is optimized. Optimum value of source resistance, R_o, is given by (Motchenbacher and Fitchen, 1973):

$$R_0 = \left[\beta_o (2r_{bb'} r_e + r_e^2) \right]^{\frac{1}{2}} \qquad (3.35)$$

where β_o = short circuit current gain

$r_{bb'}$ = base - spreading resistance

r_e = emitter resistance

$$R_e = \frac{0.026}{I_C} \text{ at } 290^o \text{ K}$$

When $r_{bb'}$ is negligible:

$$R_o = \frac{0.026}{I_C} \sqrt{\beta_o} \qquad \{3.36\}$$

Investigation of Eq. {3.36} indicates that increasing I_C will reduce the optimum source resistance required. Looking back from the base of transistors Q_2 and Q_3 in Fig. 3.5, a low source resistance value of about 400 ohms is seen, due to R_3 and R_5 respectively. Thus, to optimize the noise performance of Q_2 and Q_3 they should be operated with a high collector current. Since the amplifier bias conditions require that these transistors operate at a relatively high current level of 1mA, meeting this low noise criterion does not pose any problem.

A limit to the optimum noise figure, F_{opt}, attainable froma transistor is defined by (Motchenbacher and Fitchen, 1973):

$$F_{opt} = 1 + \frac{1}{\sqrt{\beta_o}} \qquad \{3.37\}$$

From this expression, we observe that a transistor with high current gain will produce less noise.

The 2N3117 transistor used as Q_2 and Q_3 is a hermetically sealed planar transistor having low leakage currents (10nA maximum). Contours of constant narrow band noise figure shown in Fig. 3.8 indicate a favorable noise figure of near 4 dB when the device is operated with a 1mA collector current and a 400 ohm source resistance. A plot

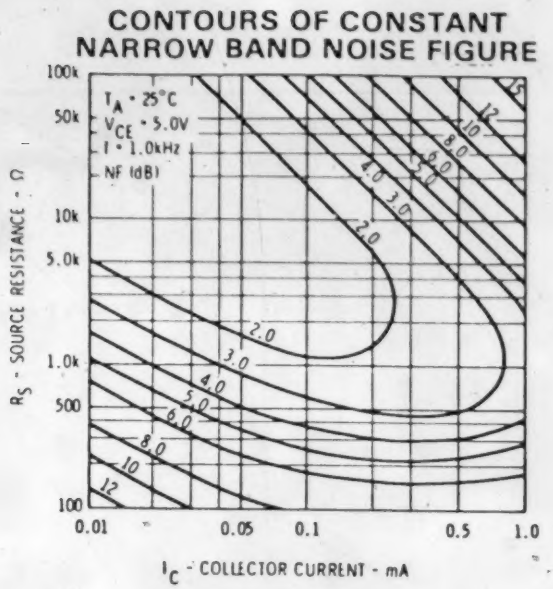

Figure 3.8 Contours of constant narrow band noise figure for the Fairchild 2N3117 bipolar transistor.

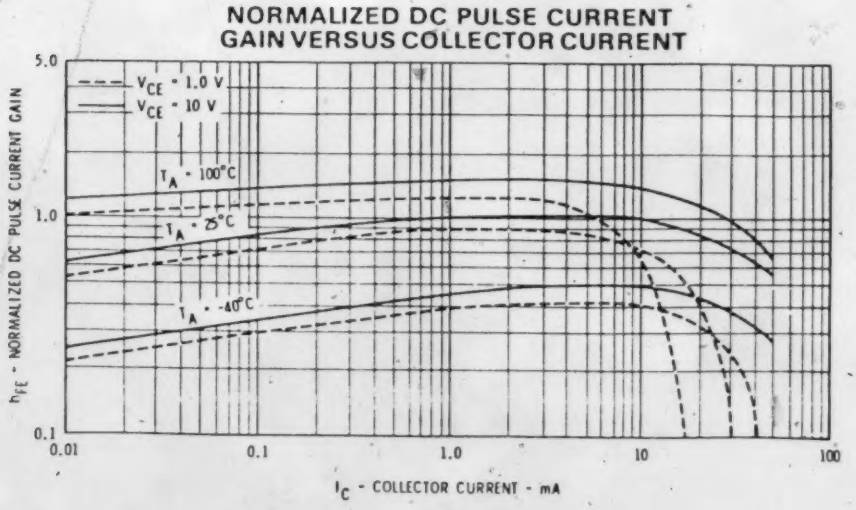

Figure 3.9 Normalized current gain vs. collector current for the Fairchild 2N3117 bipolar transistor.

of normalized current gain versus collector current of the 2N3117 is shown in Fig. 3.9. The figure shows that the transistor will operate near its maximum current gain, which is about 650, when its collector current is 1mA, making it a desirable selection as far as Eq. {3.37} is concerned.

The Operational Amplifiers 0A1 and 0A2

In addition to the normal semiconductor noise mechanisms, the operation of an operational amplifier can be seriously affected by any popcorn noise generated in its initial and second stages. This popcorn noise, also referred to as burst noise, has a power spectral density with a $1/f^{\alpha}$ function with $1<\alpha\leq 2$ and most often $\alpha = 2$. The cause of the noise is believed to be from the modulation of junction current by defects in the junction, such as a metallic precipitate (Motchenbacher and Fitchen, 1973).

The noise performance of an IC op-amp depends a lot on the manufacturing process and not solely on the type number. The RCA CA6741T is a low-noise linear IC op-amp that is free of popcorn noise as a result of improved processing developments and rigid popcorn noise inspection criteria. This selection process also assures good overall excess noise performance as well.

3.7 Amplifier Noise Measurements

The inherent internal noise of an amplifier may be represented using equivalent noise voltage and current

generators at the amplifier input (Motchenbacher and Fitchen, 1973). Such a representation is illustrated in Fig. 3.10 using a zero impedance noise voltage generator, E_n, in series with the input port and an infinite impedance noise current generator, I_n, in parallel. The noise voltage generator, E_t, represents the thermal noise of the signal source.

According to superposition theory the mean squared input noise of the amplifier, E_i^2, may be obtained as:

$$E_i^2 = E_{In}^2\Big|_{\substack{E_n=0\\E_t=0}} + E_{En}^2\Big|_{\substack{E_t=0\\I_n=0}} + E_{Et}^2\Big|_{\substack{E_n=0\\I_n=0}} \qquad \{3.38\}$$

To determine the affect of I_n we short circuit E_n and E_t, giving:

$$E_{In}^2 = I_n^2 R_s^2 \frac{Z_i^2}{(R_s+Z_i)^2} \qquad \{3.39\}$$

Similarly, to determine the affect of E_n we short circuit E_t and open circuit I_n, so that:

$$E_{En}^2 = E_n^2 \frac{Z_i^2}{(R_s+Z_i)^2} \qquad \{3.40\}$$

And finally, to determine E_t we short I_n and open I_n, giving:

$$E_{Et}^2 = E_t^2 \frac{Z_i^2}{(R_s+Z_i)^2} \qquad \{3.41\}$$

Applying Eq. {3.38} we obtain the sum:

$$E_i^2 = (E_t^2+E_n^2+I_n^2R_s^2)\frac{Z_i^2}{(R_s+Z_i)^2} \qquad \{3.42\}$$

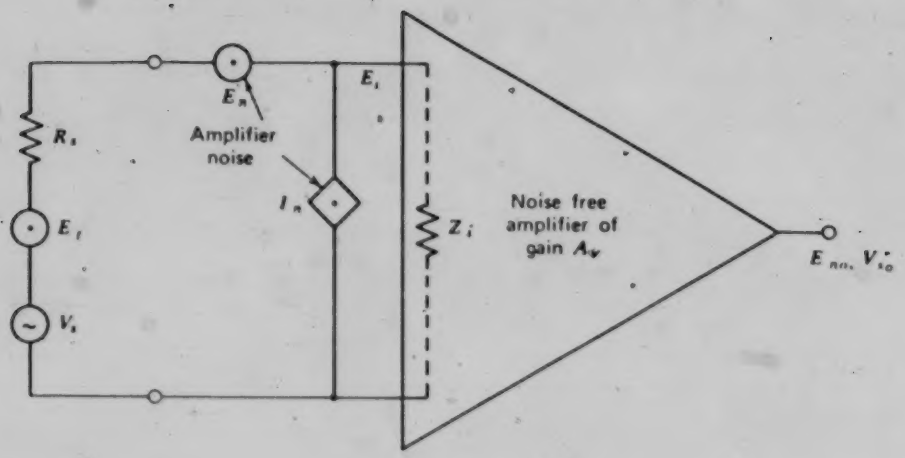

Figure 3.10 Amplifier equivalent input noise model (Motchenbacher and Fitchen, 1973).

From Eq. {3.42} we obtain a definition of the mean squared equivalent input noise, E_{ni}^2, as:

$$E_{ni}^2 = E_t^2 + E_n^2 + I_n^2 R_s^2 \qquad \{3.43\}$$

Measurement of E_{ni}, E_n and I_n

The thermal noise E_t of the source can be determined quite easily by application of the Nyquist relation, Eq. {3.31}.

The second term E_n is independent of source resistance, R_s, so that if R_s is set close to zero Eq. {3.43} becomes:

$$E_{ni}^2 = E_n^2 \qquad \{3.44\}$$

Thus, if the amplifier output noise, E_{no}, is measured while $R_s = 0$ the noise voltage E_n can be obtained from:

$$E_n = \frac{E_{no}}{A_v} \qquad \{3.45\}$$

where A_v is the amplifier voltage gain.

Since $I_n R_s$ is directly proportional to R_s, while E_t is proportional to the square root of R_s, the $I_n R_s$ term of Eq. {3.43} will eventually dominate if R_s is sufficiently large. How large R_s must be of course depends on the amount of noise current, I_n, generated by the amplifier. Consequently, if the amplifier output noise, E_{no}, is measured while R_s is very large the noise current I_n can be obtained from:

$$I_n = \frac{E_{no}}{G_v} \frac{1}{R_s} \qquad \{3.46\}$$

where G_v is the system gain taking the source resistance

into account. If the thermal noise contribution is still significant for large values of R_s its effect must be subtracted.

A measurement of equivalent input noise, E_{ni}, may be accomplished using the sine wave measurement technique (Motchenbacher and Fitchen, 1973 and Vandenbrock, 1969). The system voltage gain, G_v, is measured at midband with a sine wave signal and then the rms noise voltage, E_{no}, at the amplifier output is measured. Finally, the equivalent input noise is calculated as:

$$E_{ni} = \frac{E_{no}}{G_v} \qquad \{3.47\}$$

The equivalent input noise of the REU amplifier was measured with the hook-up shown in Fig. 3.11. The value of the source resistance, R_s, was varied from 50 ohms to 10 M ohms to determine its influence. The sine wave generator was inserted in series with R_s and the amplifier so that the system gain, G_v, and frequency bandwidth could be measured. With this set-up the signal level could be set significantly higher than the noise levels to be measured. Finally, the output noise is measured on the ouput meter and the equivalent input noise is calculated using Eq. {3.47}. Thermal noise levels of the source resistance are determined using the bandwidth measurements in conjunction with Eq. {3.31}.

The meter used was a true rms reading meter (Bruel and Kjaer, Type 2409) with a bandwidth 50 times

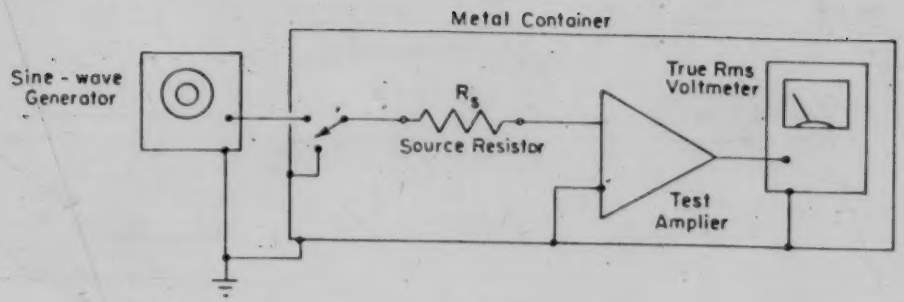

Figure 3.11 Amplifier noise measurement circuit.

greater than the output noise bandwidth. The meter, amplifier and source resistor were electrically shielded and connected to ground via a single line to prevent outside interference and ground loops from entering into the measurements.

A plot of E_{ni} versus R_s for the REU amplifier is shown in Fig. 3.12. Separate curves for the individual functions E_t, E_n and I_nR_s are also included to illustrate their relative contributions to the equivalent input noise. At low values of R_s, E_n alone is important and exhibits a value of 1.6 microvolts. A 10 M ohm value of R_s is not sufficient to allow the I_nR_s voltage to dominate the thermal noise voltage. At R_s = 10 M ohms, values of E_{ni} = 47.9 microvolts and E_t = 30.2 microvolts were determined, thus a value for I_n is obtained using Eq. (3.43):

$$I_n = \left[\frac{E_{ni}^2 - E_t^2}{R_s^2}\right]^{\frac{1}{2}} = \left[\frac{47.9^2 - 30.2^2}{10^2}\right]^{\frac{1}{2}}$$

giving I_n = 3.7 picoamps

The point at which the E_n line intersects with the I_nR_s line at R_s = 450 K in Fig. 3.12 is also significant. At this value of source resistance the E_{ni} curve approaches closest to the E_t line, or in other words, the amplifier adds a minimum amount of noise in comparison to the thermal noise already present from the source. This obviously, from a low noise stand point, is the optimum source resistance with which to operate the amplifier.

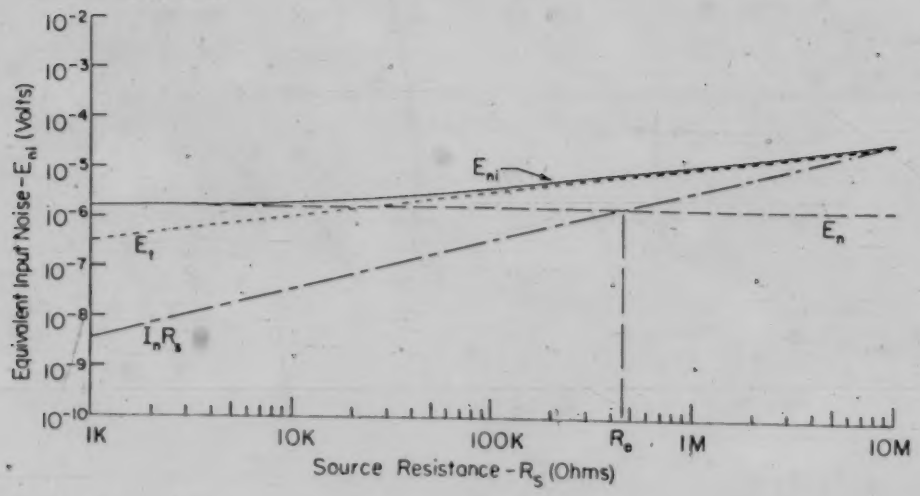

Figure 3.12 Equivalent input noise versus source resistance - REU amplifier.

A value for the optimum source resistance, R_o, may be predicted mathematically from:

$$R_o = \left. \frac{E_n}{I_n} \right|_{E_n = I_n R_s} \qquad \{3.48\}$$

$$= \frac{1.6 \times 10^{-6} \text{ v.}}{3.7 \times 10^{-12} \text{ A.}}$$

giving $R_o = 430 \text{ K } \Omega$

Since an average electrode impedance of 100 K ohms is expected, the amplifier will in fact be operating near this optimum source resistance.

Measurement of Noise Figure

A figure-of-merit for an amplifier, as far as noise is concerned, is the noise figure, NF, expressed in dB. The noise figure in terms of E_n and I_n is defined as:

$$NF = 10 \log \frac{E_{ni}^2}{E_t^2} \qquad \{3.49\}$$

A plot of NF versus R_s for the REU amplifier is shown in Fig. 3.13. As can be appreciated, the curve dips to a value of about 1.5 dB when the source resistance is about 450 K ohms, the amplifier's optimum source resistance. At this point the amplifier's noise contribution is only 20% greater than the source noise.

The optimum noise figure, NF_{opt}, that the amplifier is capable of reaching is obtained by combining Eqs. {3.49}, {3.43} and {3.31} when $E_n = I_n R_s$, giving:

$$NF_{opt} = 10 \log \left[1 + \frac{E_n I_n}{2kT\Delta f} \right] \qquad \{3.50\}$$

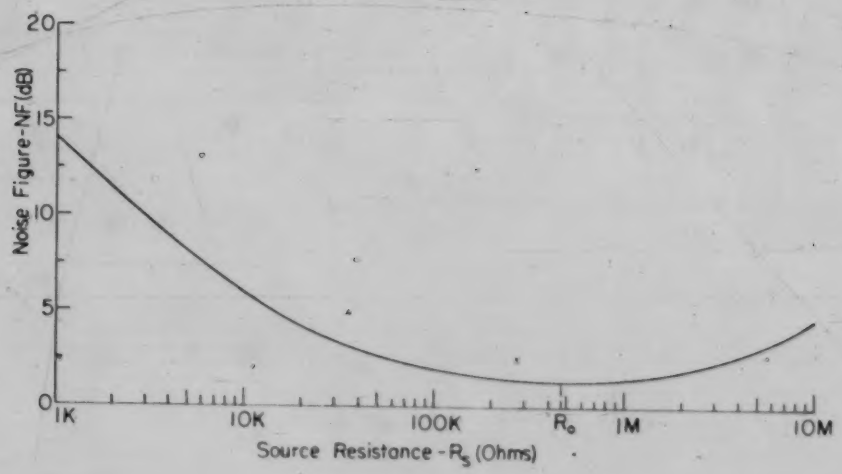

Figure 3.13 Noise figure vs. source resistance REU amplifier.

Using E_n = 1.6 microvolts and I_n = 3.7 picoamps over a measured bandwidth Δf = 5.9 K Hz gives:

$$NF_{opt} = 10 \log 1.13 = 0.53 \text{ dB}$$

We see from Fig. 3.13 that the noise figure is less than 3 dB for source resistances of value from 30 K ohms to 5 M ohms which is well within the electrode impedance limits. At 3 dB, half the amplifier output noise will be from the source.

A comparison set of E_{ni} and NF versus R_s curves measured for the Grass P15 solid state amplifier, a leading low-noise commercial physiological amplifier, is shown in Appendix II.

CHAPTER 4

AMPLIFIER RECORDING TESTS

4.1 Preparation

Limited success in obtaining reliable regeneration electrode recordings, dictated that the amplifier recording tests be made using a conventional nerve recording technique.

A unipolar measurement preparation was set up using the dorsal cutaneous nerve of a frog. As shown in Fig. 4.1, the preparation involved the use of a silver recording wire to lift the nerve out, away from the tissue saline bath, into an insulating paraffin oil layer. A second ground electrode is placed into the frog's tissue. This arrangement produced triphasic nerve action potentials when the nerve was excited using pressure contact on the skin.

4.2 Tests

Electrode impedance measurements of the set up indicated a 120 K ohm impedance with very little frequency dependence due to a small 7^{o} phase angle. This is expected because of the relatively large size of the electrode wire.

The nerve impulse recordings were made inside a screened room with a 5 mm length of nerve raised into the paraffin. Oscilloscope snapshots of several superimposed triggered impulses are shown in Fig. 4.2(a), (b) and (c). Fig. 4.2(d) is a snapshot of the amplifier output noise envelope using the 120 K ohm electrode as the source. When

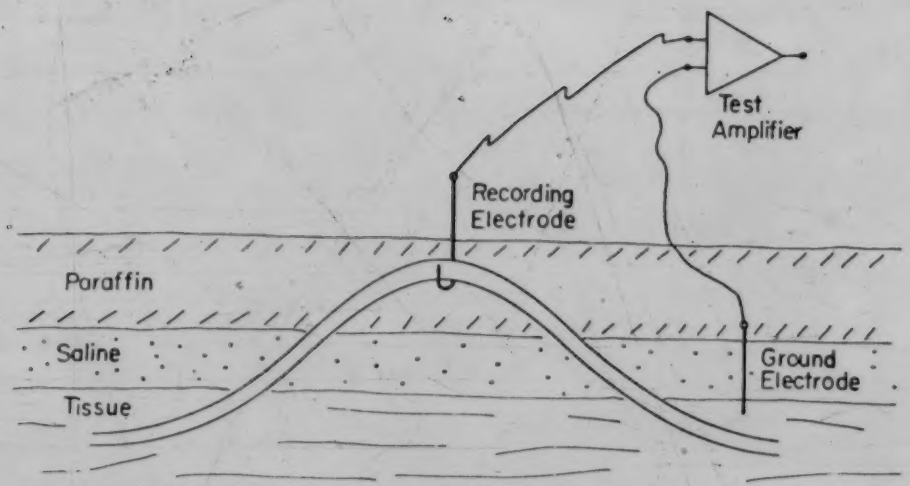

Figure 4.1 Recording preparation showing dorsal cutaneous nerve lifted into paraffin onto a silver recording electrode.

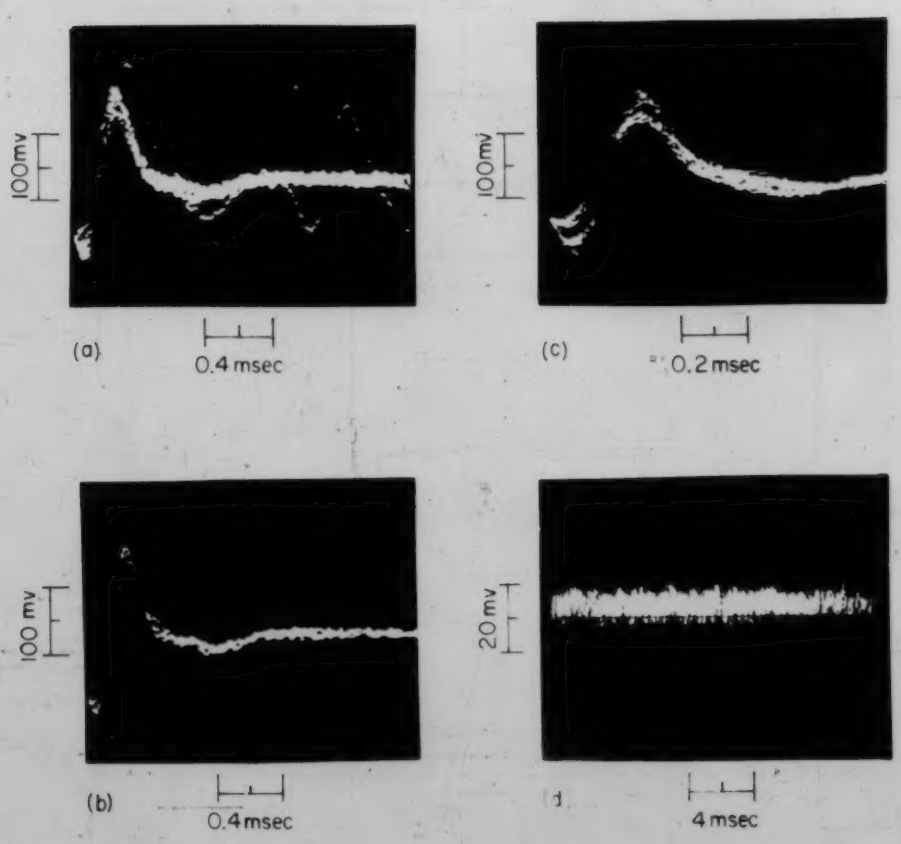

Figure 4.2 Amplifier test recordings.

divided by the amplifier gain, the envelope represents an equivalent input noise voltage of 3.3 microvolts rms. Comparison snapshots using a commercially constructed Grass P15 physiological amplifier are included in Appendix II.

Unshielded tests outside of the screened room near a.c. power operated equipment and open flourescent lighting, created some 60 Hz interference problems, as shown in Fig. 4.3. The tests were done with 10 inches of unshielded connecting leads between the FET and the amplifier main body. Outside interference however, proved to be a result of pick-up from the nerve preparation and not the FET leads. Tests with the source shielded and the FET leads unshielded did not detect any significant increase in noise levels above the amplifier's internal noise level.

4.3 Suggestions for Interference Noise Level Reduction

When the REU - amplifier hook-up is made, one of the electrode leads can be used to serve as an "indifferent electrode." This electrode will be inactive as far as signal is concerned, but will have the same impedance level as theother active leads. The indifferent electrode can then be connected to a second amplifier channel, working differentially in conjunction with the active recording amplifier to supply common mode rejection of the interference signal. A method of accomplishing this may be done by modifying the second op-amp stage, OA2, of Fig. 3.1 from that of an inverting amplifier to a differential amplifier

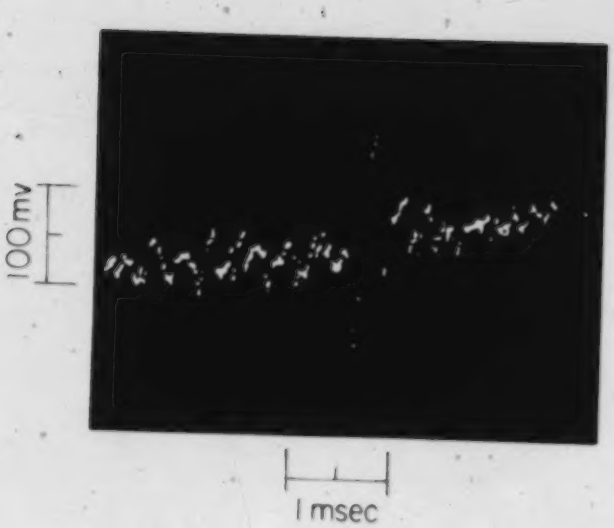

Figure 4.3 Single nerve impulse with baseline disrupted from 60 Hz external interference.

circuit as illustrated in Fig. 4.4.

With the present method, the REUs have long leads leading to the skin button. These leads will not only pick up outside 60 Hz interference but may also pick up muscle EMG activity. Long electrode leads can be avoided, if the electrodes are fabricated with semi-conductor FET chips bonded to the electrode leads in close proximity, adjacent to the electrode nerve channel. In this manner, the long noisy electrode leads could be replaced with the interference free FET leads.

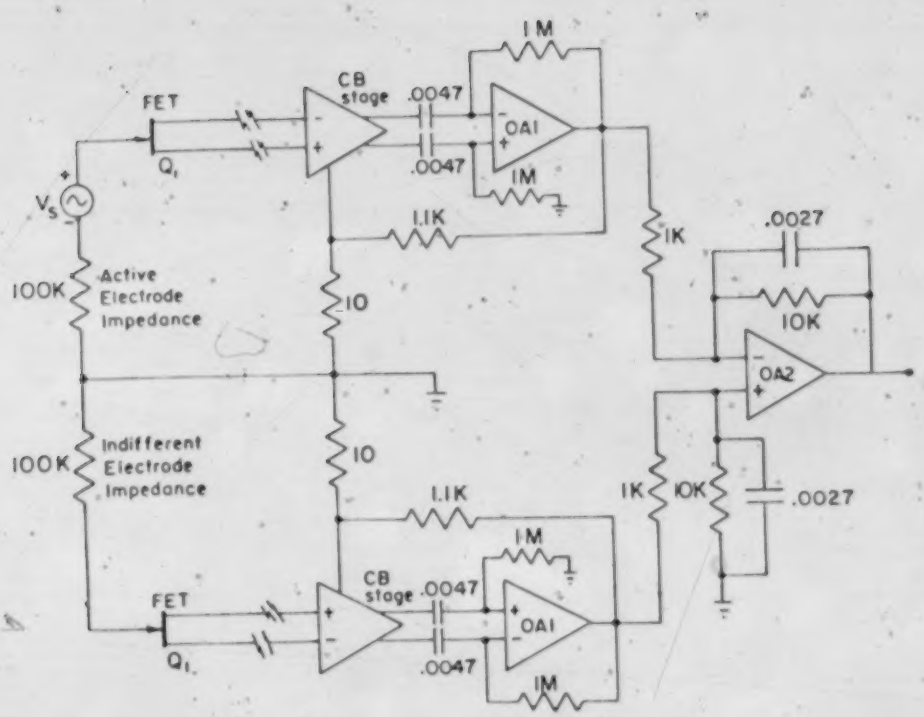

Figure 4.4 Suggested circuit to give common mode rejection.

CHAPTER 5

DISCUSSION

5.1 Electrode Impedance

A model illustrating the impedance effects of the electrode double-layer was derived in the theory of Chapter 1. It has been developed from theory collected from articles and textbooks on electrochemistry, and from other investigations in physiological electrode theory and fabrication techniques.

The frequency response plots of the impedance characteristic measurements obtained for the regeneration electrodes, indicate a -10 dB/decade variation of impedance magnitude with increasing frequency over a bandwidth of 10 Hz to 10 K Hz. This characteristic was shown to be analogous to the impedance properties of an R-C transmission line (Fig. 1.6). It was concluded that this effect can be attributed to the diffusion zone layer of the electrode interface. A method paralleling that used to derive the impedance of an R-C transmission line, was used to develop the expression for the impedance of the diffusion zone under linear (low excitation voltage) conditions (Eq. 1.38). V. Pollak, (1974a), using a computer model simulating the electrode impedance network equivalent to the one used in this thesis, has successfully matched the appropriate parameters and physical constants for platinum electrodes in 0.9% NaCl to produce frequency-response characteristics for

electrodes by computer calculation. The computated characteristics closely paralleled with his measured characteristics, thus demonstrating the model to be viable.

Comparison of the REU impedance characteristics presented in Chapter 2 with those obtained for silver electrodes by another investigator (V. Pollak, 1974b) are quite favourable, even though a more accurate technique employing an a.c. bridge was used for measurement by the latter. The measurements made by V. Pollak on polished silver electrodes of considerably larger diameter (0.254 cm) than that of the REUs (0.076 cm), indicate impedance levels near 900 K ohms at very low frequencies and near 2 K ohm at high frequencies. The characteristic diffusion layer -10 dB/decade slope is also clearly present.

Measurements of the REU impedances at 1 K Hz, indicated a wide variation in magnitudes from device to device (ranging from 25 K ohms to 1 M ohm with an average near 100 K ohms). A greater degree of impedance consistency would be preferable from the point of view of obtaining predictable recordings and optimizing common-mode rejection of interference signals during differential recording. Also, as far as low noise operation of the amplifier is concerned, the electrode resistance should be maintained as near as possible to the optimum source resistance of the amplifier (section 3.7), particularly if the REU signal levels prove to be small. The greatest

factors found to affect impedance consistency are the surface area and surface roughness of the electrode. Impedance testing also proved to be an asset when checking for electrode faults such as fractured insulation causing leakage currents to the grounded electrolyte.

5.2 Amplification Method

A multi-channel arrangement is required to obtain simultaneous recordings from the REU. However, the cramped condition of the space near the device socket prohibits the clustering of large amplifying units around it. The Bergveld amplification method was therefore adopted, as it offered a satisfactory, interference free, means of being able to dislocate the small input FET from the amplifier circuit proper, without using shielded cables, to a remote position at the REU socket. Furthermore, the relatively small number of circuit components in the amplifier allow it to be miniaturized quite readily. Manufacturing techniques in hybrid integrated circuits such as beam lead construction are also available to permit further miniaturization. Alternative approaches such as using a FET source follower at the implant site, require more components, shielded cables and extra power-supply leads, and do not offer the same capabilities of interference rejection.

Noise measurements performed on the amplifier show that when the circuit is designed using low-noise components biased to optimize their noise performance, the amplifier can perform as quietly as a leading available

commercial amplifier which is considerably larger in size (see comparison noise measurements of the GRASS P15 pre-amplifier, Appendix II).

Further improvements of the amplifier circuit can be suggested, should future requirements indicate their need. To maximize the interference rejection properties of the FET drain and source leads, the bipolar transistors Q_2 and Q_3 of Fig. 3.1 can be replaced by matched pair low-noise transistors. Doing so will have two advantages: (1) the emitter resistance of Q_2 and Q_3 will be equal, thus allowing the condition of Section 3.2 to be satisfied more precisely, (i.e., the source resistance will equal the drain resistance) and (2) the current gains of Q_2 and Q_3 will be equal making the output voltage equality, $V_{01} = -V_{02}$, met more exactly. This will, in effect, allow whatever common mode signal that has escaped cancellation thus far to undergo further cancellation by the differential op-amp, OA1.

The search for a better FET could be continued to optimize further the following: it may be possible to locate a FET that, while satisfying the circuit bias conditions, will need less drain current and give a higher "ohmic" region trans-conductance. This will mean less noise and more gain.

If greater temperature stability is required for conditions other than the present experimental conditions of the room-temperature laboratory, a scheme could be

developed to make the emitter currents of Q_2 and Q_3 equal to the currents through their base biasing diodes. This will allow changes in the forward biased base - emitter junction to track changes in the diode junctions.

At this point in time, it is not known whether or not the FET gate leakage-current of 2nA is sufficient to disrupt the action-potential activity of regenerated nerve fibres. If future tests reveal this to be a problem, a FET will have to be obtained with a lower, less disruptive, leakage level.

BIBLIOGRAPHY

Barker, G. C. (1961). Faradaic Rectification. Trans. Symp. Electrode Processes. Yeager, E. (Ed), John Wiley, New York.

Barker, G. C. (1966). The Equivalent Circuit for the Electrical Double Layer. J. Electroanal. Chem. 12, 495.

Bergveld, P. (1968). New Amplification Method for Depth Recording. IEE Transactions on Biomedical Engineering, BME-15, 102.

Bockris, J'OM. (1951) Overpotential. Electrical Phenomena at Interphases. Butler, J. A. V. (Ed), Methuen, Chpt. 8.

Bockris, J'OM. (1954). Electrode Kinetics. Modern Aspects of Electrochemistry. Bockris and Conway, (Ed), Butterworths Scientific Pub., London.

Bockris, J. and Reddy, A. (1970 Modern Electrochemistry. Plenum Press, New York.

Breyer, B. and Bauer, H. H. (1963). Alternating Current Pology raphy and Tensammetry in Chemical Analysis. Interscience Publishers of John Wiley, V. 13.

Butler, J. A. V. (1951). Electrical Potential Differences and Their Origin. Electrical Phenomena at Interfaces. Butler, (Ed) Methuen and Co., London, Chpt. 1.

Damaskin, B. B. (1967). The Principles of Current Methods for the Study of Electrochemical Reactions. McGraw Hill Book Co.

Davies, C. W. (1967). Electrochemistry. London George Newves Ltd., Chpt. 9.

Delahay, P. (1965). Double Layer and Electrode Kinetics. Interscience Pub. of John Wiley.

de Levie, R. (1967). Electrochemical Response to Porous and Rough Electrodes. Advances in Electrochemistry and Electrochemical Engineering. Interscience of John Wiley.

Graeme, J. G.; Tobey, G. E. and Huelsman, L. P. (Editors). (1971) Burr-Brown: Operational Amplifiers. McGraw-Hill Book Co.

Grahame, D. C. (1947). The Electrical Double Layer and the Theory of Electrocapillarity. Chem. Rev. 41, 441.

Grahame, D. C. (1952). Mathematical Theory of the Faradaic Admittance. J. Electrochem. Soc. Dec. 1957.

Mannard, A.; Stein. R. B. and Charles, D. (1974). Regeneration Electrode Units: Implants for Recording from Peripheral Nerve Fibres in Freely Moving Animals. Science, 183, 547.

Margaretha, S. and Sluyters, J. H. (1970). Sine Wave Methods in the Study of Electrode Processes. Electroanalytic Chemistry. Bard, A. J. (Ed), Marcel Dekker Inc., New York, V. 4.

Millman, J. and Halkias, C. C. (1972). Integrated Electronics: Analog and Digital Circuits and Systems. McGraw Hill Book Co.

Mohilner, D. M. (1966). The Electrical Double Layer, Pt. 1 in Electroanalytical Chemistry. Bard, A. J. (Ed), Marcel Dekker Inc., N.Y., V. 1.

Motchenbacher, C. D. and Fitchen, F. C. (1973). Low-Noise Electronic Design. John Wiley and Sons.

Novosel'skii, I. M. (Sept. 1968). Determination of the Parameters of Equivalent Electrode Circuits. Soviet Electrochem. V. 4, N. 9, P. 971.

Parsons, R. (1954). Equilibrium Properties of Electrified Interfaces. Modern Aspects of Electrochemistry. Bockris, J. (Ed). Butterworths Scientific Pub., London.

Parsons, R. (1961). The Structure of the Electrical Double Layer and its Influence on the Rates of Electrode Reactions. Advances in Electrochemistry and Electrochemical Engineering. Delahay, P. (Ed), Interscience Pub. of John Wiley, V. 1.

Parsons, R. (1970). Faradaic and Non-Faradaic Processes. Advances in Electrochemistry and Electrochemical Engineering. Delahay and Tobias (Eds), Interscience Pub. of John Wiley, V. 7.

Pollak, V. (1974a). Computation of the Impedance Characteristic of Metal Electrodes for Biological Investigations. Medical and Biological Engineering. 12, 460.

Pollak, V. (1974b). Impedance Measurements on Metal Needle Electrodes. Medical and Biological Engineering, 12, 606.

Randles, J. E. B. (1947). Kinetics of Rapid Electrode Reactions. Discussions of the Faraday Society, No. 1. P. 11.

Robinson, D. A. (June, 1968). The Electrical Properties of Metal Microelectrodes, Proc. I.E.E.E. 56, No. 6.

Stein, R. B. and Wong, R. (1970). The Amplitude of Nerve Impulses Extracellularly from Restricted Lengths of Nerve. Physiology Canada, 2, 29.

Stein, R. B. and Pearson, K. G. (1971). Predicted Amplitude and Form of Action Potentials Recorded from Unmyelinated Nerve Fibres, J. Theor. Biol. 32, 539-558.

Vanden Broek, J. (1969). Noise Figure as a Measure of Amplifier Performance. News from Transidyne General Corporation. V1. No. 11.

APPENDIX I

BRIDGE APPROXIMATION

APPENDIX I

The network of Fig. 2.1 may be simplified to the following:

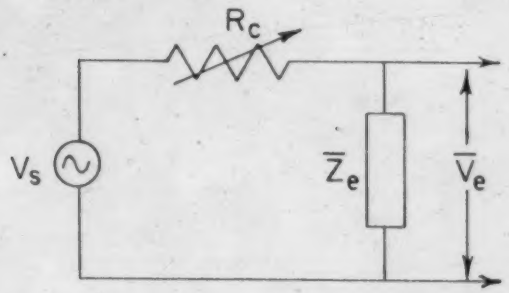

where $\overline{Z}_e$ is the electrode impedance. Analysis will demonstrate that:

$$\frac{\overline{V}_e}{\overline{V}_s} = \frac{\overline{Z}_e}{R_c + \overline{Z}_e}$$

If R_c is adjusted so that:

$$\left|\frac{\overline{V}_e}{\overline{V}_s}\right| = \frac{|\overline{Z}_e|}{|R_c + \overline{Z}_e|} = \frac{1}{2}$$

$$\text{then} \quad |R_c + \overline{Z}_e| = 2|\overline{Z}_e| \qquad \{1\}$$

Expressing $\overline{Z}_e$ in polar form, we write:

$$\overline{Z}_e = Z_e \ (\cos \theta + j \sin \theta) \qquad \{2\}$$

where θ is the phase angle between the real and imaginary parts. Solution of Eqs. {1} and {2} reduces to solving the quadradic:

$$3 Z_e^2 - 2 Z_e R_c \cos\theta - R_c^2 = 0$$

$$\text{or} \quad Z_e = \frac{R_c}{\sqrt{\cos^2\theta + 3} - \cos\theta} \qquad \{3\}$$

Tabulated solution of (3) is as follows:

θ	Z_e
0^o	R_c
30^o	$0.93\ R_c$
45^o	$0.86\ R_c$
60^o	$0.77\ R_c$
70^o	$0.70\ R_c$
80^o	$0.64\ R_c$
90^o	$0.56\ R_c$

which demonstrates the error involved should the electrode being measured contain significant capacitance. Phase angle measurements of some electrodes, using a vector impedance meter, showed phase angles as high as 60^o at low frequencies, but generally phase angles of less than 45^o were measured. Since the object here was to gain only an approximate idea of how the regeneration electrodes would behave, the error involved was considered tolerable, expecially when compared to day to day shifts in electrode impedance. Other methods of electrode impedance measurements can be used but these are not without disadvantage as well.

The above mentioned bridge can be modified to reduce the error involved by keeping R_c fixed at some value much greater than the expected electrode impedance (Robinson, 1968). This value may be as high as 1000 megaohms when large impedance electrodes are being measured. Thus, with $R_c >> Z_e$ expression (1) reduces to:

$$\left|\frac{V_e}{V_s}\right| = \left|\frac{Z_e}{R_c}\right|$$

The output voltage measured across the electrode then is directly proportional to the impedance magnitude. High values of R_c unfortunately create noise problems which must be overcome by using larger input voltages that may put the electrode into non-linear operation. Also, shunt capacitances impose serious limitations on higher frequency measurements.

A vector impedance meter gives an instant readout of both impedance magnitude and phase angle, and can be used over a wide range of frequencies. To overcome noise problems involved with high magnitude impedance, however, the instruments introduce progressively larger input voltages which drive an electrode well into non-linear operating regions.

A well shielded a.c. bridge arrangement is probably the best means of electrode impedance measurement. Accurate measurements using bridge circuits have already been accomplished by Pollak, 1974, and are proving to be reliable.

APPENDIX II

COMPARATIVE MEASUREMENTS ON THE GRASS P15 PHYSIOLOGICAL AMPLIFIER

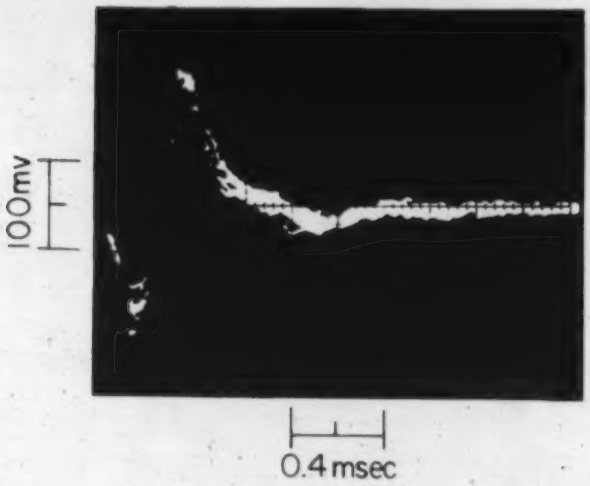

Figure 1 Oscilloscope photograph of several superimposed nerve impulses.

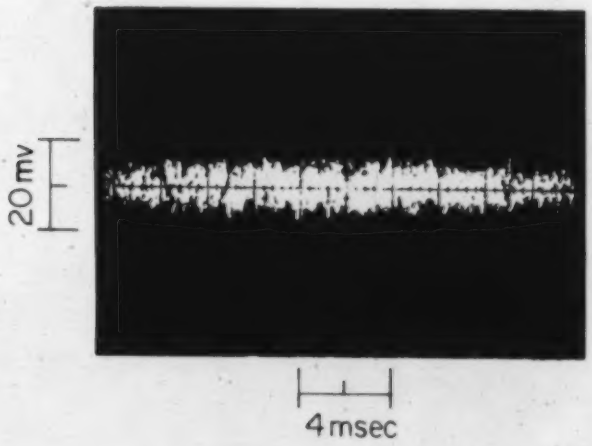

Figure 2 Amplifier output noise envelope.

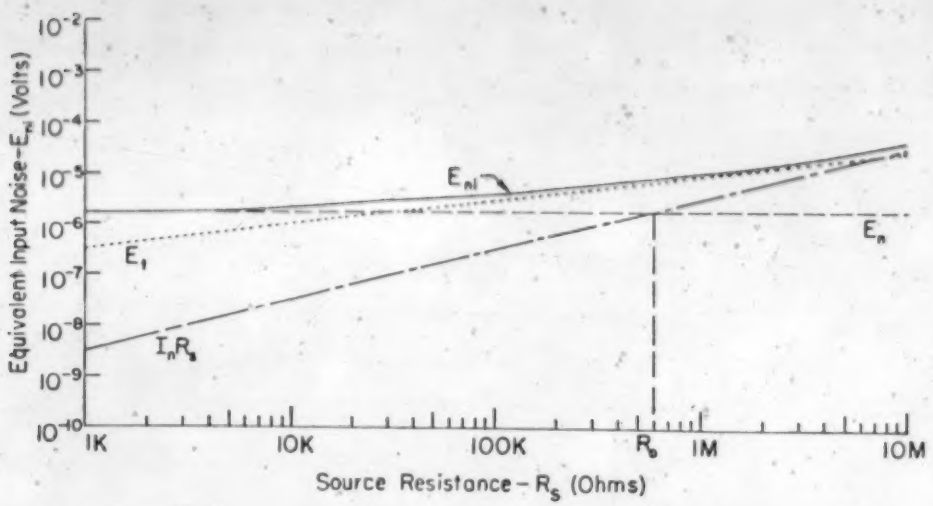

Figure 3 Equivalent input noise versus source resistance Grass P15 amplifier.

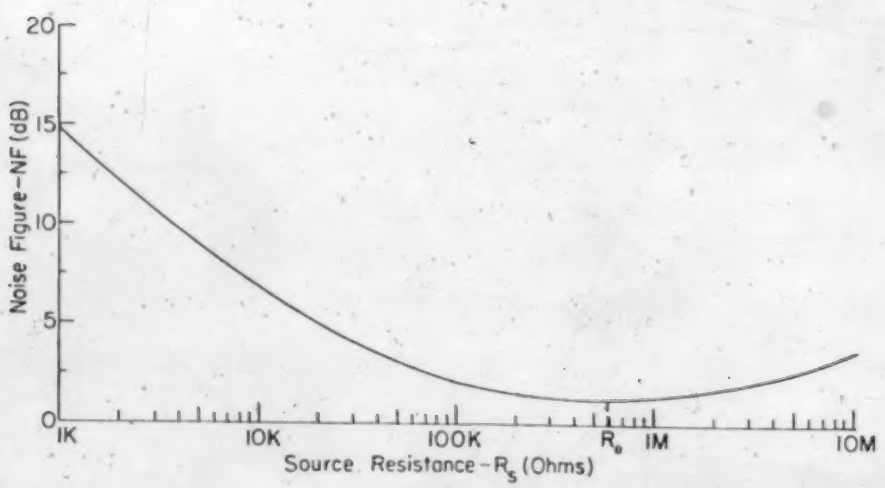

Figure 4 Noise figure versus source resistance Grass P15 amplifier.